ANNUAL REVIEWS

Annual Review of Chemical and Biomolecular Engineering

Active Colloids as Models, Materials, and Machines

Kyle J.M. Bishop,[1] Sibani Lisa Biswal,[2] and Bhuvnesh Bharti[3]

[1]Department of Chemical Engineering, Columbia University, New York, NY, USA; email: kyle.bishop@columbia.edu

[2]Department of Chemical and Biomolecular Engineering, Rice University, Houston, Texas, USA

[3]Cain Department of Chemical Engineering, Louisiana State University, Baton Rouge, Louisiana, USA

Annu. Rev. Chem. Biomol. Eng. 2023. 14:1–30

First published as a Review in Advance on March 17, 2023

The *Annual Review of Chemical and Biomolecular Engineering* is online at chembioeng.annualreviews.org

https://doi.org/10.1146/annurev-chembioeng-101121-084939

Keywords

nonequilibrium, active matter, self-propelled, colloidal assemblies

Abstract

Active colloids use energy input at the particle level to propel persistent motion and direct dynamic assemblies. We consider three types of colloids animated by chemical reactions, time-varying magnetic fields, and electric currents. For each type, we review the basic propulsion mechanisms at the particle level and discuss their consequences for collective behaviors in particle ensembles. These microscopic systems provide useful experimental models of nonequilibrium many-body physics in which dissipative currents break time-reversal symmetry. Freed from the constraints of thermodynamic equilibrium, active colloids assemble to form materials that move, reconfigure, heal, and adapt. Colloidal machines based on engineered particles and their assemblies provide a basis for mobile robots with increasing levels of autonomy. This review provides a conceptual framework for understanding and applying active colloids to create material systems that mimic the functions of living matter. We highlight opportunities for chemical engineers to contribute to this growing field.

1. INTRODUCTION

The remarkable capabilities of living cells and their assemblies represent the pinnacle of chemical engineering design. Informed by Darwinian evolution, these biological systems harness dissipative processes such as chemical reactions, mass transport, and fluid flow to perform diverse functions that foster their survival. Swimming microorganisms navigate structured environments in pursuit of chemical food; epithelial cells assemble to form adaptive, self-healing barriers; muscle tissue coordinates molecular machines to drive macroscopic motions. These and other dynamic functions (1) cannot be achieved at thermodynamic equilibrium but instead require flows of energy and matter to sustain material organization in space and time. As we seek to create synthetic materials that mimic the functions of living matter, we must therefore advance our ability to understand, design, and control nonequilibrium systems in which dissipative flows act to animate material structures. Here, we argue that progress toward this long-standing goal can benefit from a systems-level perspective that combines knowledge of thermodynamics, chemical kinetics, and transport phenomena in pursuit of targeted capabilities. In short, to create lifelike material systems, we need chemical engineering.

Humbled by the complexity of living matter, we focus on comparatively simple model systems that use external energy inputs to direct the structure and dynamics of material components. In this context, colloidal dispersions of solid particles in liquid media provide convenient building blocks on scales spanning 0.1–10 μm that can be imaged directly by optical video microscopy. These materials have a venerable history as experimental models of condensed matter, in which colloidal particles play the role of "big atoms" (2) that interact and assemble to form condensed phases such as crystalline solids as well as disordered liquids, glasses, and gels. Such passive particles can be energized by catalytic reactions or external fields to create active colloids that move autonomously and assemble spontaneously to form dynamic structures free from the constraints of thermodynamic equilibrium (3–5). With this freedom comes new challenges of understanding nonequilibrium materials and designing their behaviors for useful purposes.

Beyond their value as model systems, the study of active colloids is motivated by applications in microrobotics (6, 7) and smart materials (8). As mobile robots, self-propelled particles promise to navigate microstructured environments to manipulate matter and information in targeted locations that are otherwise inaccessible. In the context of human health, such capabilities would enable new strategies for precision diagnostics, therapeutic delivery, and noninvasive surgery. Other targeted application areas include environmental remediation and material repair, whereby colloidal robots seek and degrade toxic compounds or heal structural defects. The realization of these outstanding goals will require significant progress in our ability to design active colloids with intelligent behaviors conditioned on their local environments. For example, microrobots designed for autonomous cargo retrieval should be able to swim through structured fluids, navigate local gradients (e.g., chemotaxis), capture targeted cargo, and return home without external intervention or control. While living cells perform these basic tasks routinely, synthetic robots have the potential to function also in extreme environments hostile to life.

As materials, assemblies of active colloids leverage new principles of organization to enable temporal control over material structure and achieve new functions prohibited at equilibrium. The promise of these active materials is best illustrated by biological examples such as microtubules within the cytoskeleton of a living cell (9). These self-assembled structures are both mechanically strong and dynamically reconfigurable due to coupling with chemical reactions. Such chemically fueled assembly processes enable dissipative functions such as force generation and mechanical actuation underlying cell motility. Likewise, colloidal particles energized by chemical fuels or external fields can organize to form dynamic assemblies of tunable structure, size, and morphology.

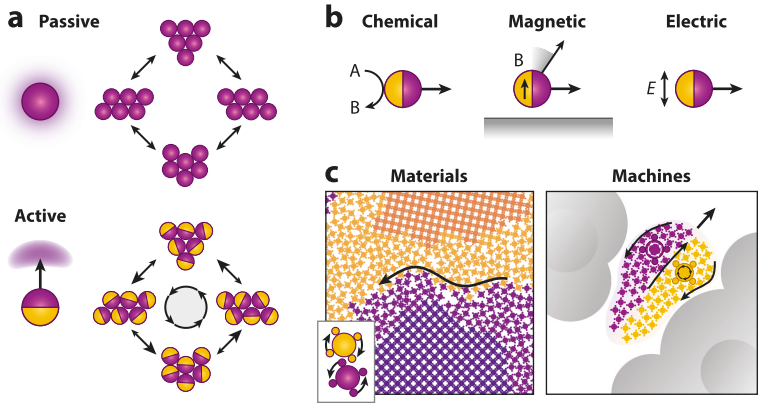

Figure 1

(*a*) Comparing active and passive colloids. Active colloids use external energy inputs to break time-reversal symmetry and drive steady currents prohibited at equilibrium. Such currents enable (*left*) directed particle motion and (*right*) assembly cycles. (*b*) Three flavors of active colloids powered by chemical fuels (Section 4), magnetic fields (Section 5), and electric currents (Section 6). The different actuation strategies use nonconservative forces and/or time-varying potentials (Section 3) to propel particle motion. (*c*) In addition to their value as model systems, active colloids provide a basis for the dynamic self-assembly of materials and machines. (*Left*) Colloidal spinners phase separate to form rotating crystals and fluids (10). (*Right*) Colloidal cells of active components move and deform to navigate structured environments (11).

The functions of such active materials—like those of living matter—derive not only from their composition and structure but also from the dissipative processes that animate their components.

In this review, we discuss recent progress on three types of active colloids powered by chemical fuels, magnetic fields, and electric currents, highlighting opportunities for chemical engineers to contribute to their understanding and application (**Figure 1**). All of these materials operate outside of equilibrium; however, that label does little to distinguish them among the many flavors of nonequilibrium systems. Therefore, we begin with a primer on colloids at equilibrium and the different ways in which equilibrium assumptions can be broken. We focus on systems where thermodynamic fluxes (e.g., chemical reactions, electric currents) and/or time-varying potentials (e.g., due to oscillating magnetic fields) drive the motion and assembly of colloidal particles. For each of the three classes, we briefly review the mechanisms of propulsion at the single-particle level and discuss their consequences for the collective behaviors of particle ensembles. Throughout our discussion, we make connections between current research questions and chemical engineering fundamentals in the hope of stimulating our colleagues and students to join in the pursuit of active materials with lifelike capabilities. Overall, the purpose of this review is to provide the background knowledge and conceptual framework for understanding and applying the growing variety of active colloids and their assemblies.

2. COLLOIDS AT EQUILIBRIUM

To better appreciate the distinguishing features of active colloids, it is instructive to compare them with similar materials at thermodynamic equilibrium. Here, we describe how the conditions required for equilibrium place significant restrictions on the structure and dynamics of colloidal dispersions. By relaxing these conditions, we enable new behaviors such as time-varying structure, directed motion, and force generation, among others.

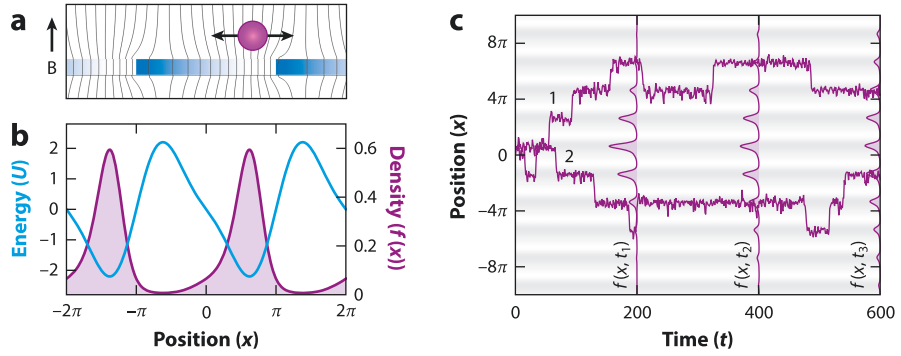

Figure 2

Brownian motion of a single particle on an asymmetric periodic potential. (*a*) Schematic illustration of an experimental realization in which a superparamagnetic sphere diffuses above a patterned magnetic substrate in an applied field (18). (*b*) Equilibrium distribution $f(x)$ (*purple*) as a function of position x for the potential $V(x) = -A[\sin(kx) - (1/4)\sin(2kx)]$ (*blue*) with amplitude $A = 2k_BT$. (*c*) Transient particle position x versus time t starting from $x(0) = 0$. The solid curves denote two solutions $x(t)$ of the Langevin equation; the distributions denote the Fokker–Planck solution $f(x, t)$ at successive times. We adopt units in which the wave number k, diffusivity $D = k_BT/\xi$, and thermal energy k_BT are each one (for details, see the **Supplemental Material**).

Supplemental Material >

2.1. Equilibrium Structure: Colloidal Self-Assembly

Dispersions of rigid colloidal particles in simple liquids provide useful experimental models to validate and visualize key concepts of equilibrium statistical mechanics. Due to differences in scale between the particles (0.1–10 μm) and the liquid molecules (0.1–1 nm), it is convenient to adopt a coarse-grained perspective that considers only the positions and orientations of the particles—collectively denoted **X**. At thermodynamic equilibrium, the probability density of finding the particles in a particular configuration is given by the Boltzmann distribution, $f(\mathbf{X}) \propto \exp(-V(\mathbf{X})/k_BT)$, where V is the system energy, k_B is the Boltzmann constant, and T is the temperature of the surrounding fluid. Particle configurations with lower energy are more likely to be observed at equilibrium (**Figure 2*a*,*b***).

This familiar result has important implications for material design. At equilibrium, material structure—that is, the organization of colloidal building blocks in space—is independent of time and is specified uniquely by the energies of different particle configurations. In practice, the energy V is often approximated by summing over pairwise interactions (12–14) among neighboring particles to enable predictive simulations of colloids at equilibrium. By engineering the particles and their interactions, one can direct the spontaneous formation of targeted, low-energy configurations—for example, the long-elusive diamond lattice (15). In this way, equilibrium statistical mechanics provides a unifying framework for the programmable self-assembly of colloidal structures (16).

2.2. Equilibrium Dynamics: Brownian Motion

Langevin equation: stochastic differential equation describing system dynamics due to deterministic and fluctuating forces

Even at equilibrium, colloidal particles do not sit motionless in their minimum energy configuration but rather jiggle incessantly due to frequent collisions with the surrounding molecules. This so-called Brownian motion leads to fluctuations in the particle configuration that serve to achieve and maintain the Boltzmann distribution described above. The stochastic dynamics of colloidal particles is well described by the relevant Langevin equation, which accounts for conservative forces that act to lower the system energy as well as fluctuating forces that originate in the liquid

bath (17). Owing to the particles' small size, the effects of particle inertia are often negligible, and the resulting dynamics are overdamped.

As a specific example, consider the Brownian motion of a single particle on an asymmetric periodic potential (**Figure 2**). The particle position $x(t)$ fluctuates within the low-energy wells of the potential, hopping occasionally to neighboring wells (**Figure 2*c***). An alternative perspective of Brownian motion shifts the focus from a single fluctuating trajectory $x(t)$ to the transient probability distribution $f(x, t)$ described by the Fokker–Planck equation (17). En route to equilibrium, this distribution evolves by diffusion and convection to occupy the kinetically accessible, low-energy regions of the configuration space (**Figure 2*c***).

Equilibrium dynamics satisfy an important symmetry known as detailed balance, which relates the forward and reverse transition rates between any states x_1 and x_2 at equilibrium:

$$f(x_2, t' \mid x_1, t) f_{\text{eq}}(x_1) = f(x_1, t' \mid x_2, t) f_{\text{eq}}(x_2). \quad 1.$$

Here, $f_{\text{eq}}(x)$ is the equilibrium distribution and $f(x_2, t'|x_1, t)$ is the conditional probability density for finding the system in state x_2 at time t' given that it is in state x_1 at time t. Net currents are strictly prohibited in systems at equilibrium. Thus, despite the asymmetric potential, the Brownian particle in **Figure 2** diffuses with equal probability in both the positive and negative x directions.

These complementary descriptions—the Langevin and Fokker–Planck equations—are readily generalized to any number of dynamical variables. For a collection of N colloidal particles, the effects of viscous friction are described by the resistance tensor, which relates the hydrodynamic forces and torques on the particles to their linear and angular velocities at low Reynolds numbers (19). For shape anisotropic particles (20), this tensor depends on their positions and orientations; it describes how the motion of one particle contributes to the forces and torques on its neighbors. Such hydrodynamic interactions (21) play a critical role in determining the collective dynamics of colloidal particles driven from equilibrium.

Fokker–Planck equation: partial differential equation describing time evolution of the system distribution function

Detailed balance: principle forbidding net currents at equilibrium

Hydrodynamic interactions: coupling of force–velocity relationships among neighboring particles

3. MANY ROUTES TO NONEQUILIBRIUM

The assumptions underlying the equilibrium systems outlined above can be broken in different ways to create different types of nonequilibrium materials. Many material systems remain out of equilibrium only because they relax slowly relative to experimental timescales [e.g., colloidal glasses (22) and gels (23)]. The dynamics of such systems may be well described by the equilibrium formalism outlined above. However, when relaxation to equilibrium is sufficiently slow, the system remains kinetically trapped within local regions of phase space that depend strongly on system preparation and history. Understanding this type of nonequilibrium is critical to achieving kinetic control over the self-assembly of colloidal materials but is not our present focus.

Alternatively, systems open to the addition or removal of particles can be driven and maintained out of equilibrium by interactions with multiple-particle reservoirs. When particles are systematically added to one part of the system and removed from another, their diffusive dynamics produce a net current of particles from source to sink, thereby disrupting the equilibrium distribution. This type of nonequilibrium relating thermodynamic forces and fluxes (24) should be familiar to chemical engineers as the colloidal analog of molecular transport, whereby chemical potential gradients drive particle fluxes in open systems. Here, we consider closed systems with a constant number of colloidal building blocks to which energy is continuously supplied.

Active colloids are driven from equilibrium by time-varying potentials and/or nonconservative forces induced by dissipative fluxes. The system energy $V(\mathbf{X}, t)$ may vary in time due to externally applied fields, thereby prohibiting relaxation to equilibrium. Alternatively, the forces that act to alter the particle configuration may be indescribable as gradients of a scalar potential, $-\nabla V(\mathbf{X})$.

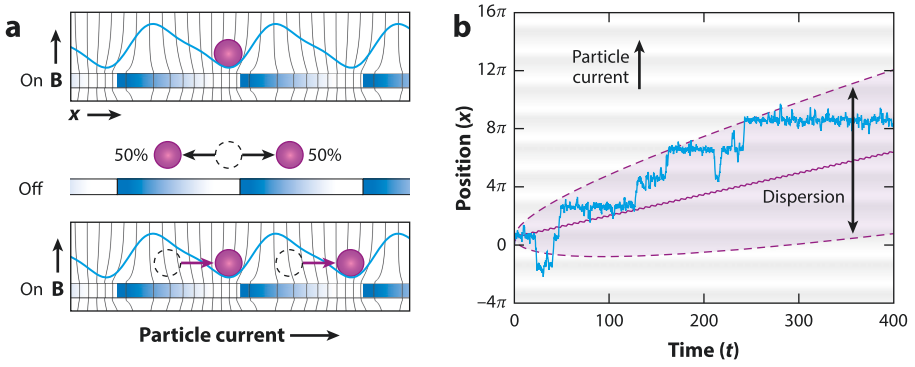

Figure 3

Directed motion of a Brownian particle in a time-oscillating, asymmetric potential. (*a*) Schematic illustration of a flashing ratchet. When the potential is off, the particle diffuses to the left or right with equal probability. Subsequent application of the potential results in net particle migration from left to right. (*b*) Simulated particle dynamics in the potential, $V(x,t) = A[-\sin(kx) + (1/4)\sin(2kx)][1 + \cos(\omega t)]$, with amplitude $A = 3\,k_B T$ and frequency $\omega = 1\,k^2 D$. The mean particle position (*purple curve*) increases linearly in time; the standard deviation about the mean (*shaded region*) increases as $t^{1/2}$. The blue curve shows a single realization of the particle's stochastic trajectory. We adopt units in which the wave number k, diffusivity $D = k_B T/\xi$, and thermal energy $k_B T$ are each one (see the **Supplemental Material**).

Supplemental Material >

Such nonconservative forces derive from dissipative processes associated with microscopic degrees of freedom (e.g., that of ions or solvent molecules) omitted in our coarse-grained formulation of colloidal dynamics. Below, we use simple toy models to illustrate some basic features of these two classes of nonequilibrium systems.

3.1. Time-Varying Potentials

Active colloids based on time-varying potentials use external fields (e.g., magnetic, electric) to modulate the system energy in time $V(\mathbf{X}, t)$—for example, by changing interparticle interactions. The resulting particle configuration is inherently time dependent and can no longer satisfy the Boltzmann distribution. Specifically, we consider the special case of time-periodic forcing in which the system energy oscillates with a constant frequency ω. Such systems evolve in time to a periodic steady state, which can exhibit interesting behaviors such as anomalous diffusion, steady currents, and work generation.

Figure 3 illustrates some of these effects for a single particle diffusing on a time-periodic energy landscape. Notably, the particle dynamics is governed by the same Langevin and Fokker–Planck equations as an equilibrium system with the exception of the potential energy, which is now time-dependent $V(x, t)$. Interestingly, when the oscillating potential is spatially asymmetric, the particle's stochastic motion becomes biased in a preferred direction. This "flashing ratchet" uses the oscillatory drive to sustain dissipative particle currents that can be harnessed to perform mechanical work (25). Such currents are greatest when the frequency of the drive is comparable to the particle relaxation time (here, $\omega \sim k^2 D$). By contrast, low-frequency drives lead to temporal modulation of the equilibrium distribution; high-frequency drives create an effective time-averaged potential. In either limit, particle currents cease and equilibrium-like behavior is restored.

3.2. Nonconservative Forces

Active colloidal systems can also be driven from equilibrium by nonconservative forces—that is, by forces that cannot be described in terms of potential gradients. This type of nonequilibrium has

long been appreciated in colloidal rheology, in which applied shear flows induce hydrodynamic forces on dispersed particles that drive their motion and alter their microstructure (26). Substituting these forces into the N-body Langevin equation leads to dissipative dynamics that violates the condition of detailed balance among other characteristics of thermodynamic equilibrium.

More generally, nonconservative forces in colloidal dispersions derive from dissipative processes such as electric currents, solute fluxes, and chemical reactions. An electric field drives the steady migration of charged particles by electrophoresis (27); a solute gradient drives similar motion by diffusiophoresis (28). In contrast to gravitational sedimentation, these phoretic motions (29) are force free, like those of swimming microorganisms, which use internal mechanisms to push or pull against their viscous surroundings (30). The dynamics of force-free particles cannot be described within the equilibrium formalism outlined above (see Section 4). Nevertheless, low-symmetry particles subject to external gradients are typically constrained to "swim" up or down the direction of the field.

By contrast, self-propelled particles move even through isotropic environments due to local gradients they create—for example, using chemical reactions (Section 4). Self-propulsion can be modeled by a nonconservative force that drives particle translation at a constant speed U along a direction that fluctuates due to rotational diffusion (**Figure 4**). The dynamics of this active Brownian particle (ABP) is controlled by a Péclet number, $\mathrm{Pe} = U/(D_t D_r)^{1/2}$, where D_t and D_r are diffusion coefficients for particle translation and rotation, respectively. This dimensionless parameter describes the ratio between the so-called run length U/D_r and the characteristic particle size $(D_t/D_r)^{1/2}$ (31). Particles with strong activity ($\mathrm{Pe} \gg 1$) travel many particle lengths in a common direction before their orientation is disrupted by rotational diffusion.

Like the flashing ratchet above, the ABP model exhibits nonequilibrium behaviors such as enhanced diffusion due to particle activity, deviations from Boltzmann statistics, and steady particle currents in asymmetric environments. At long times, self-propelled particles exhibit diffusive motion with an effective diffusivity that increases with particle activity (**Figure 4*b***). Such particles violate the condition of detailed balance (Equation 1), which allows for rectified motion on an

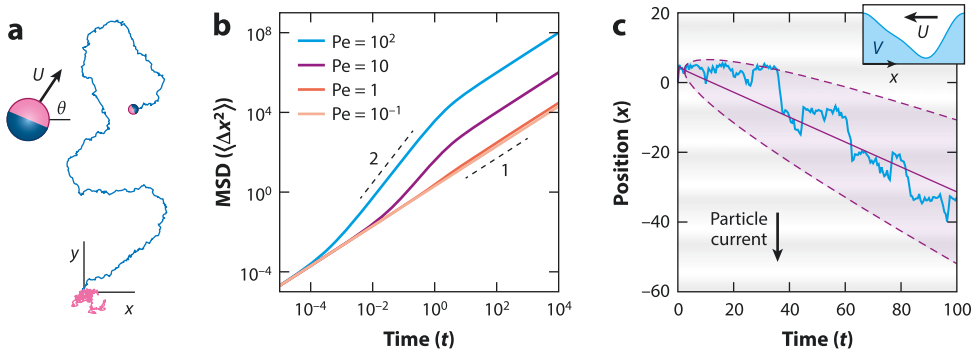

Figure 4

Dynamics of an ABP in two dimensions. (*a*) Simulated trajectories of a passive particle (*pink*) and an ABP (*blue*) with Péclet number $\mathrm{Pe} = 10$. (*b*) MSD versus time. Particle dynamics for $\mathrm{Pe} \gg 1$ shows three regimes: passive diffusion at short times ($\mathrm{MSD} \propto t$), ballistic motion at intermediate times ($\mathrm{MSD} \propto t^2$), and active diffusion at long times ($\mathrm{MSD} \propto t$). (*c*) An ABP exhibits directed motion on an asymmetric potential with amplitude $A = 20\, k_B T$, wave number $k = 0.5(D_t/D_r)^{1/2}$, and $\mathrm{Pe} = 10$. The drift velocity U is directed toward smaller potential gradients. We adopt units in which the rotational diffusivity D_r, translational diffusivity D_t, and thermal energy $k_B T$ are each one (for details, see the **Supplemental Material**). Abbreviations: ABP, active Brownian particle; MSD, mean squared displacement.

Supplemental Material >

asymmetric periodic potential (**Figure 4*c***). More generally, active colloids harness energy flows from their environment to break time-reversal symmetry and power-dissipative dynamics with no counterpart in equilibrium systems (32).

3.3. Three Flavors of Active Colloids

In the following sections, we introduce three classes of active colloids powered by chemical fuels (Section 4), time-varying magnetic fields (Section 5), and electric currents (Section 6). Like the toy models above, these experimental systems use nonconservative forces and/or time-varying potentials to propel particle motion and direct active particle assemblies. Catalytic reactions at the surface of asymmetric colloids create local gradients that propel particle motion via phoretic effects such as diffusiophoresis. Such self-propelled motions and the interactions they induce lead to dynamic behaviors described by nonconservative forces that challenge intuitions built on the study of equilibrium materials. Time-varying magnetic fields modulate dipolar interactions between magnetic colloids to create fluctuating energy landscapes that direct material assemblies. Nonreciprocal fields (e.g., rotating fields) induce local torques that drive particle rotation and fluid flows to create active colloidal fluids, vortices, and swarms. Electric fields act on particles and the surrounding ions to drive particle dynamics that combine effects due to time-varying potentials and nonconservative forces. We review the principles underlying these active particles and highlight examples from the literature that illustrate their rich phenomenology.

4. CHEMICALLY FUELED, SELF-PROPELLED COLLOIDS

Flagellated bacteria use chemical fuels to rotate helical filaments and propel their motion through viscous environments at speeds of several body lengths per second (30, 33). In 2004, these self-propelled biocolloids were joined by the first synthetic analogs, known as catalytic nanomotors (34). Similar in size to bacteria (2 μm long, 0.4 μm across), these bisegmented rods of platinum (Pt) and gold were observed to swim spontaneously through solutions of hydrogen peroxide fuel at speeds of ∼10 μm/s. Following this pioneering discovery, researchers have come to understand the mechanisms by which the catalytic consumption of chemical fuels at the particle surface can be used to propel its motion. Briefly, reactions at the surface of an asymmetric particle create gradients in the concentrations of chemical species, in the electric potential, in the temperature, and so forth. These local reaction-induced gradients create stresses at the particle–fluid interface that drive fluid flow and particle motion known as phoretic transport (29). In this section, we review common mechanisms of phoretic self-propulsion (35, 36) and discuss how interactions between phoretic particles break action–reaction symmetry to create active colloidal assemblies.

4.1. Phoretic Self-Propulsion

For specificity, we focus our discussion of phoretic self-propulsion on another well-studied experimental system: the Pt-coated Janus sphere in hydrogen peroxide (31) (**Figure 5**). Polystyrene microspheres coated on one hemisphere by a thin layer of Pt exhibit self-propelled motion when dispersed in hydrogen peroxide solutions (31). The particles' stochastic trajectories are well described by the ABP model combining Brownian motion and linear self-propulsion (**Figure 5*b***). However, the detailed mechanism(s) by which catalytic reactions propel particle motion remains uncertain despite a growing body of experimental evidence on the effects of peroxide concentration (31), particle size (37), ionic strength (38, 39), solution pH (39), and confining boundaries (40–42).

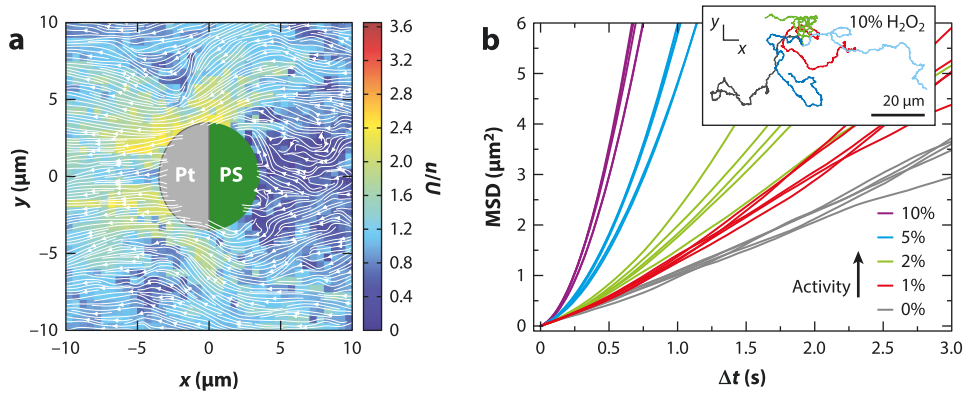

Figure 5

Self-propulsion of Pt-Janus spheres in H_2O_2. (*a*) Fluid flow field around a freely swimming, active sphere measured experimentally using particle tracking velocimetry. The 7 μm Pt-PS sphere is dispersed in 10 wt% H_2O_2; the fluid speed u is scaled by the swimming speed U. (*b*) MSD versus lag time Δt for 1.6 μm Pt-PS spheres swimming above a glass substrate in H_2O_2 solutions of increasing concentration (31). (*Inset*) Particle trajectories for 10 wt% H_2O_2. Abbreviations: MSD, mean squared displacement; PS, polystyrene. Panel *a* adapted from Reference 43 (CC BY 4.0). Panel *b* adapted from Reference 31.

4.1.1. Neutral solute self-diffusiophoresis. The consumption (production) of chemical reactants (products) at the surface of an asymmetric particle creates local gradients in the solute concentration directed tangent to the particle–fluid interface (**Figure 6*a***). Due to molecular interactions between the solute(s) and the particle surface, there exists a thermodynamic driving force for fluid flow near the interface that acts to increase (decrease) the frequency of favorable (unfavorable) interactions. These gradient-induced flows and the resulting particle motion are known as diffusio-osmosis and diffusiophoresis, respectively (29).

For a neutral solute, the apparent slip velocity $\mathbf{v}_s$ at the particle surface is linearly proportional to the surface concentration gradient as $\mathbf{v}_s = \mu \nabla_s C$, where the magnitude and sign of the mobility μ depend on the interaction potential between the solute and the particle–fluid interface. For hard-sphere solutes (29), the mobility is related to the solute radius a and the fluid viscosity η as $\mu = a^2 k_B T/2\eta$ [e.g., $\mu \approx 1.4 \times 10^{-14}$ m^5/(mol·s) for O_2 in water at room temperature]. The asymmetric production of solute at the particle surface leads to self-propelled motion with a characteristic velocity $U \sim \alpha\mu/D$, where α is the solute flux and D is the solute diffusivity (35). For the Pt-catalyzed decomposition of hydrogen peroxide [$\alpha \approx 0.01$ mol O_2/(m^2·s) in 10% H_2O_2], the predicted speed of self-phoretic propulsion is only ~0.07 μm/s—considerably slower than the ~20 μm/s observed in experiments (39). Despite its widespread use in models of active colloids (44–47), diffusiophoresis based on neutral solutes has not been established as the dominant propulsion mechanism for experimental systems of self-propelled colloids.

4.1.2. Ionic self-diffusiophoresis. For reaction-induced gradients of ionic solutes, it is necessary to consider the electrical aspects of the particle–fluid interface. Using the standard electrokinetic model (27), one can show that the apparent slip velocity due to a surface gradient in the concentration of a binary $z{:}z$ electrolyte is

$$\mathbf{v}_s = -\mu_i \nabla_s \ln C, \quad \text{with} \quad \mu_i = \frac{\varepsilon}{\eta}\frac{k_B T}{ze}\left(\beta\zeta + \frac{4k_B T}{ze}\ln\cosh\frac{ze\zeta}{4k_B T}\right), \qquad 2.$$

Diffusiophoresis: migration of a colloidal particle in a concentration gradient

where ε is the fluid permittivity, e is the elementary charge, $\beta = (D_+ - D_-)/(D_+ + D_-)$ is the dimensionless diffusivity contrast between cation and anion, and ζ is the zeta potential at the

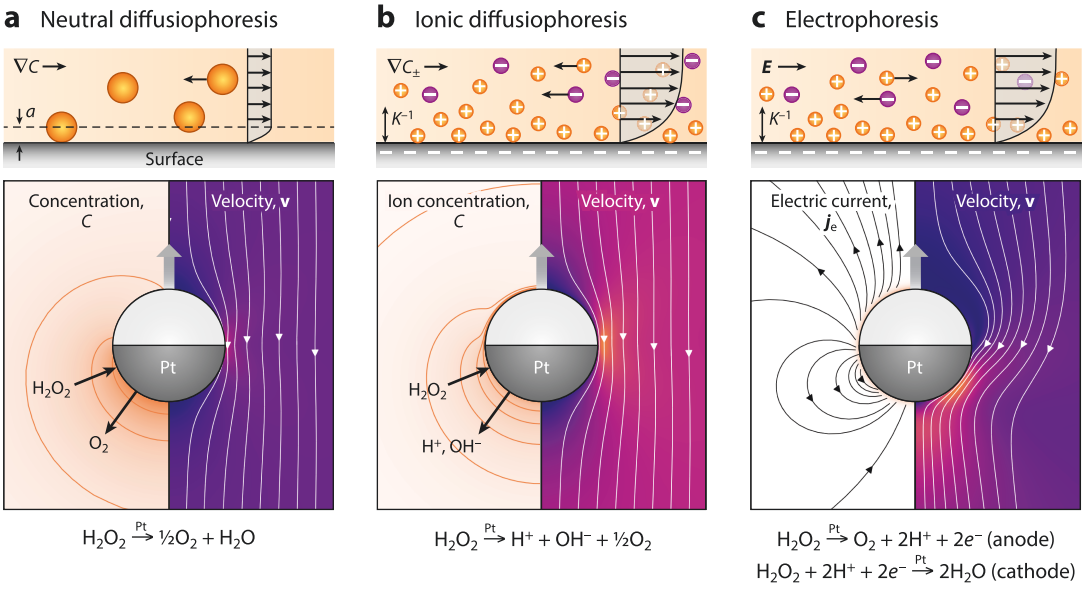

Figure 6

Three phoretic mechanisms for the self-propulsion of Pt-Janus spheres in H_2O_2 solutions. (*a*) In neutral solute self-diffusiophoresis, the catalytic production of O_2 leads to concentration gradients and fluid flow due to repulsive, excluded-volume interactions with the particle surface. (*b*) In ionic self-diffusiophoresis, reaction-induced gradients in the ion concentration drive flow at the negatively charged surface due to electro-osmosis despite the competing effects of chemiosmosis. (*c*) In self-electrophoresis, electrochemical reactions at the Pt surface drive electric currents through the electrolyte from anode to cathode; the associated electric field acts on ionic charge in the double layer to drive flow. The plots show (*left*) simulated concentration profiles and (*right*) fluid velocity fields for the three models (for details, see the **Supplemental Material**).

Supplemental Material >

particle surface (48). The diffusiophoretic mobility μ_i includes two additive contributions. The first describes electro-osmosis due to the electric field accompanying the ambipolar diffusion of ions with different diffusion coefficients. The second describes chemiosmosis due to electrostatic interactions between ions and the charged surface. Notably, the slip velocity induced by ionic solutes is proportional to the gradient of the log concentration rather than the concentration itself (28). As a result, large driving forces are achieved as the local salt concentration approaches zero.

Figure 6*b* shows a possible mechanism for the propulsion of the Pt-Janus sphere based on the catalytic production of H^+ and OH^- from hydrogen peroxide fuel (49). Diffusion of these ions from the Pt hemisphere occurs at different rates ($\beta = 0.27$), thereby generating an electric field directed toward the Pt cap. When the particle surface is negatively charged ($\zeta < 0$), the ion-induced field drives fluid flow toward the cap, which propels particle motion in the opposite direction. Notably, this model reproduces (at least qualitatively) several experimental observations for Pt-Janus spheres in hydrogen peroxide—specifically, that the propulsion velocity increases with decreasing particle size (37), decreases with increasing salt concentration (38, 39), and reverses direction upon changing the sign of the zeta potential (39).

In addition to heterogeneous reactions at the Pt surface, ionic gradients and the resulting diffusiophoretic flows can be influenced by homogeneous reactions in solution. In particular, the association of H^+ and OH^- to form water occurs over a finite length scale, ~100 nm, on which the rates of ion association and diffusion compete (50, 51). In the absence of added salt, this reaction–diffusion length is comparable to the Debye length, which describes the thickness of the electric

double layer. These length scales are sensitive to the pH of the peroxide solution, which provides a basis for pH-dependent control over the propulsion velocity. With realistic parameter estimates, this model predicts particle velocities that agree qualitatively with experimental observations (49) (see the **Supplemental Material**).

Supplemental Material >

4.1.3. Self-electrophoresis. Hydrogen peroxide and other chemical fuels may also participate in electrochemical reactions at the surface of catalytic particles. Such reactions drive electric currents through the surrounding electrolyte from anodic to cathodic regions on the particle surface (52). Within the charge-neutral electrolyte outside the electric double layer, these currents are accompanied by electric fields that propel particle motion by electrophoresis. For thin double layers, the apparent slip velocity at the particle surface due to an electric field $\mathbf{E} = -\nabla\phi$ is approximated by the Smoluchowski equation:

$$\mathbf{v}_s = -\mu_e \nabla_s \phi, \quad \text{with} \quad \mu_e = \frac{\varepsilon\zeta}{\eta}, \qquad 3.$$

where μ_e is the electrophoretic mobility (29). The current density due to electrochemical reactions is linearly related to the electric field $\mathbf{E}$ by the electrolyte conductivity σ, which increases with increasing salt concentration.

Figure 6*c* illustrates this third possible mechanism for the propulsion of Pt-Janus spheres based on self-electrophoresis, whereby anodic currents are enhanced near the Janus equator while cathodic currents are enhanced at the pole (38, 39). The resulting electric field drives electro-osmotic flow at the particle surface that propels its motion. For negative zeta potentials, the particle moves away from its Pt hemisphere at a speed $U \approx -e\alpha\varepsilon\zeta/16\eta\sigma$, proportional to the surface activity α and inversely proportional to the electrolyte conductivity σ (see the **Supplemental Material**). Notably, particle motion at speeds of ~10 μm/s is predicted for small electrochemical currents of order 1 mA/cm^2, representing a vanishing fraction of the total hydrogen peroxide consumption rate (53).

Self-electrophoresis of Pt-Janus spheres provides a plausible explanation for the observed decrease in propulsion velocity with added salt (38, 39). The existence of anodic and cathodic regions on the Pt surface can be attributed to gradients in the nanoscale thickness of the Pt layer, which have been demonstrated to alter its catalytic activity (38). Alternatively, proposed kinetic mechanisms for the electrochemical decomposition of hydrogen peroxide predict mass transfer limitations for the anodic reaction but not the cathodic reaction (51). As a result, the geometry of the Pt cap can direct the emergence of anodic and cathodic regions on an otherwise homogeneous surface. The self-electrophoretic mechanism is further supported by measurements of the velocity field around a Pt-Janus sphere (43), which is fastest on the face of the Pt cap rather than at the Janus equator (**Figures 5*a*** and **6*b*,*c***).

4.1.4. Directing motion with particle shape and patchiness. The dynamic trajectories of self-propelled colloids are constrained by particle symmetries due to geometric shape and surface patchiness. In an isotropic environment, the linear and angular velocity of self-propulsion are constant in the particle frame. These vectors are invariant to symmetry operations (e.g., reflection, rotation) that leave the particle unchanged (54). As a result, self-propelled motions in three dimensions can be organized on the basis of point group symmetries of (idealized) particles (**Figure 7*a***). In general, asymmetric particles follow helical trajectories with a specified speed, radius, pitch, and handedness. Additional symmetries—for example, a plane of mirror symmetry—constrain the allowed dynamics to achieve degenerate helical motion along circular or linear paths. In designing self-propelled particles, these symmetry arguments are useful for prohibiting undesired motions. However, a quantitative understanding of the propulsion mechanism and its

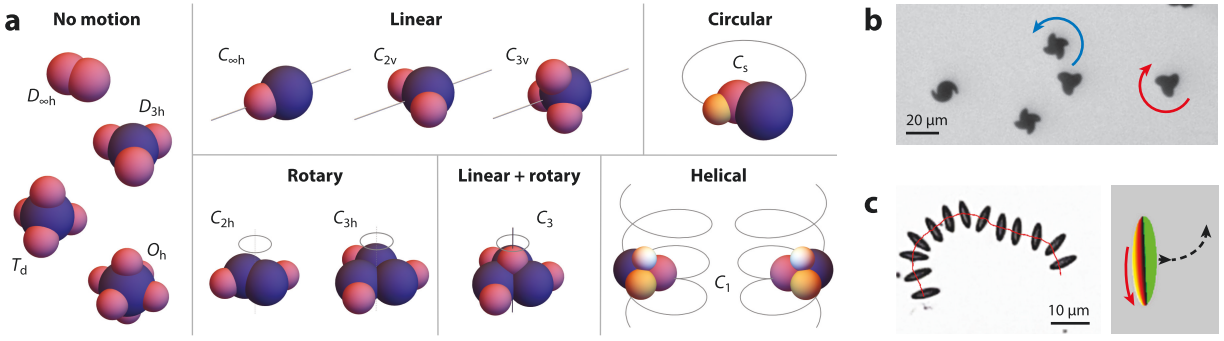

Figure 7

Particle symmetry constrains the dynamics of self-propelled colloids. (*a*) Colloidal clusters of different point symmetries are organized according to their allowed motions in an isotropic 3D environment. The details of particle motions (e.g., speed, radius, pitch, and handedness of a helical trajectory) depend on the propulsion mechanism. (*b*) Thin Pt plates with *n*-fold rotational symmetry rotate in H_2O_2 solutions with speed and direction specified by the type and extent of shape asymmetry. (*c*) Ellipsoidal particles with asymmetric Pt patches move along circular trajectories through H_2O_2 solutions. Panel *b* adapted from Reference 51 (CC BY 4.0). Panel *c* adapted from Reference 55 (CC BY-NC 3.0).

dependence on particle shape and patchiness is required to predict which motions allowed by symmetry are actually observed (51).

Near solid boundaries, the propulsion velocity is similarly constrained by the symmetry of the particle–surface complex. While motionless in an isotropic environment, active spheres can swim to or from a nearby wall due to phoretic flows on both surfaces. Anisotropic particles attracted to the wall can adopt stable orientations that direct their propulsion in the plane along linear or circular trajectories (46, 47). Importantly, the orienting effects of phoretic flows can overcome Brownian rotation to direct the motion of active particles along V-shaped grooves in a nearby surface (40, 41). Asymmetric grooves like those surrounding teardrop-shaped posts can serve to rectify motion along a preferred direction (56, 57). Freed from the constraints of detailed balance, these examples illustrate the principle that any particle motion allowed by symmetry will be observed.

The above discussion assumes that the symmetry of particle motion is uniquely determined by that of the particle and its environment. For self-phoretic propulsion, this assumption follows from the linear equations governing solute conservation and fluid flow that describe motion at low Reynolds and Péclet numbers. By contrast, at high Péclet numbers, phoretic particles may exhibit symmetry-breaking instabilities whereby the motion of an isotropic particle creates and maintains asymmetries in the local solute concentration (58). Such behavior is observed for active droplets, which swim rapidly due to Marangoni flows that accompany drop dissolution in surfactant solutions (59, 60).

4.2. Dynamic Self-Assembly of Active Colloids

Collections of active colloids organize via phoretic, hydrodynamic, and excluded-volume interactions to produce dynamic assemblies that can move, oscillate, and reconfigure as a result of continuous energy supply (**Figure 8**).

4.2.1. Active colloidal molecules. Mixtures of active colloids based on phoretic self-propulsion can assemble via long-ranged interactions to form colloidal "molecules" that break action–reaction symmetry (61, 62) (**Figure 8*a***). The nature of these interactions is illustrated by two active spheres 1 and 2 with a common radius a and respective activities α_1, α_2 and mobilities μ_1, μ_2 (61). The

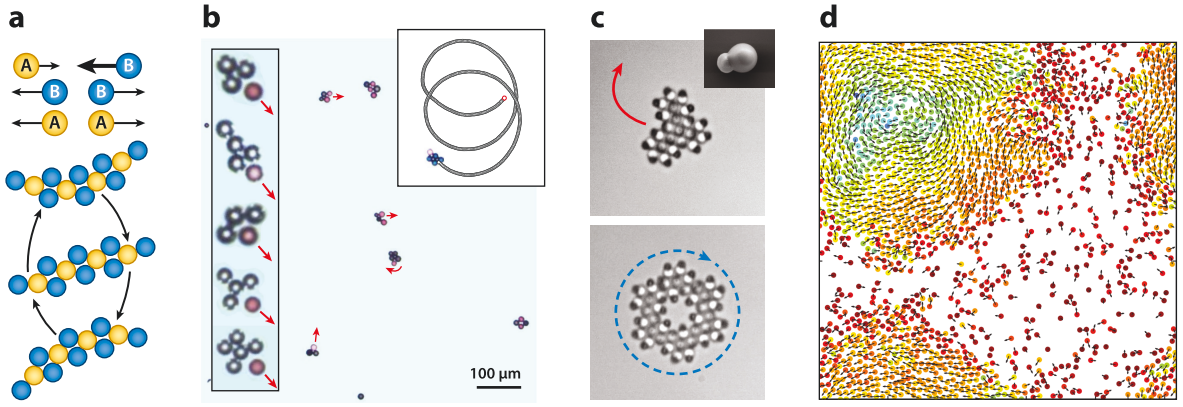

Figure 8

Active colloidal molecules, fluids, and machines. (*a*) Active colloidal molecule formed by phoretic spheres with action–reaction symmetry breaking. The active assembly forms spontaneously and oscillates steadily. (*b*) Experimental realization of active molecules assembled from binary mixtures of ion-exchange particles. (*c*) Colloidal metamachines formed by TPM–hematite heterodimers (*inset*) in H_2O_2 solution. These stable "machines made of machines" are assembled by optical traps and exhibit autonomous dynamics. (*d*) MIPS of active Brownian spheres into dense and dilute phases in three dimensions. The image shows a 2D slice with particles colored by speed (blue, slow; red, fast). Abbreviations: MIPS, mobility-induced phase separation; TPM, 3-(trimethoxysilyl)propyl methacrylate. Panel *a* adapted from Reference 62. Panel *b* adapted with permission from Reference 67, copyright 2018 American Chemical Society. Panel *c* adapted from Reference 70 (CC BY 4.0). Panel *d* adapted from Reference 71.

concentration fields produced by each sphere drive the phoretic motions of the other. In contrast to motion due to a conservative interaction potential, the velocity of sphere 1 need not be equal and opposite to that of sphere 2. The two particles attract one another when $\alpha_1\mu_2 + \alpha_2\mu_1 < 0$, forming a self-propelled doublet that moves toward sphere 1 or 2, depending on the sign of $\alpha_1\mu_2 - \alpha_2\mu_1$. These scaling arguments are further supported by analysis of the near-field hydrodynamic and chemical interactions, which reveal new behaviors such as short-ranged (long-ranged) attraction and long-ranged (short-ranged) repulsion (63). Guided by attractive phoretic interactions, active spheres are predicted to assemble into clusters that exhibit translational, rotational, and even oscillatory motion, as prescribed by their shape and composition (62, 64).

Many of these theoretical predictions have now been realized in experiments. The photocatalytic decomposition of hydrogen peroxide by hematite-containing colloids induces phoretic interactions that guide the assembly of so-called living crystals, which rapidly dissolve when the light is switched off (65). Microparticles based on ion-exchange resins exhibit attractive diffusiophoretic interactions that mediate the formation of self-propelled clusters (66). Mixtures of cationic and anionic exchange resin particles assemble to form active binary clusters that translate and rotate at different speeds (67) (**Figure 8*b***). Notably, the basic principles underlying the formation and propulsion of active phoretic assemblies apply to other mechanisms based on thermophoresis (68) and Marangoni flows (69). The diversity of active assemblies provides a basis for colloidal "machines" (11, 70) that can reconfigure among different stable structures with distinct autonomous behaviors (**Figure 8*c***).

4.2.2. Motility-induced phase separation. Even in the absence of phoretic interactions (72), the persistent motion of self-propelled particles can drive phase separation into high- and low-density phases (**Figure 8*d***). Such motility-induced phase separation (MIPS) (73) has been studied extensively using the idealized ABP model (71, 74) introduced in Section 3.2. Despite the absence of attractive interactions, ABPs condense to form liquid or crystalline phases at high Péclet

number and particle density (74). This behavior can be rationalized by a kinetic trapping mechanism whereby ABPs at the interface of the dense phase require finite time to reorient and escape to the low-density "gas" (74). If, during that time, more ABPs from the gas phase accumulate at the interface, the dense phase will grow until a kinetic balance of adsorption and desorption is achieved. Similar behaviors are observed in collections of self-propelled colloids (75); however, the influence of phoretic and hydrodynamic interactions—neglected in the ABP model—may be significant.

Directed assembly: assembly of colloids on a static energy landscape shaped by an external field

Dynamic assembly: assembly mediated by the continuous supply and dissipation of energy

Similarities between the phase separation of spherical ABPs and that of passive particles with attractive interactions motivate the pursuit of thermodynamic descriptions of these nonequilibrium systems. Active particles exert a mechanical pressure on their containers which includes an added "swim pressure" due to their self-propelled motion (76, 77). For spherical ABPs with isotropic repulsion, this pressure P depends on the bulk properties of the active fluid (e.g., the particle density ϕ) through an equation of state $P(\phi)$ analogous to that of passive fluids (76, 78). Building on this analogy, one can use the equation of state to predict the mechanical equilibrium between the dense and dilute phases $P(\phi_{\text{dense}}) = P(\phi_{\text{dilute}})$ (79). In general, however, active particles have no equation of state, and the mechanical pressure they exert on their boundaries depends on details of the wall–particle interactions (77). Analogies to equilibrium thermodynamics—though sometimes useful—are generally inadequate to describe the phase behavior of active colloids.

5. MAGNETIC FIELD–DRIVEN COLLOIDS

Static magnetic fields induce interactions among magnetic colloids that direct their assembly into structures such as chains, networks, and clusters. These stable structures correspond to local minima in the energy landscape conditioned on the applied field. By contrast, time-varying magnetic fields lead to dynamic assemblies (80) such as self-propelled crystals and rotating vortices maintained by a continuous supply and dissipation of useful energy. The collective behaviors of these systems are influenced by hydrodynamic interactions and by magnetic forces and torques. This section reviews the actuation of magnetic colloids and explores how time-varying fields enable particle assemblies on a continuum from quasi-equilibrium to emphatically nonequilibrium.

5.1. Magnetic Properties and Interactions

Directed and dynamic assembly of magnetic colloids depend on their properties, such as the magnetic moment and its response to the applied field (**Figure 9**). Magnetic interactions among such colloids contribute to the system energy, which can be modulated in time by changes in the field.

5.1.1. Classifications based on magnetic response. Magnetic colloids are composed of ferromagnetic domains such as iron oxide nanoparticles embedded within a polymer network. The magnetization of the individual domains tends to align with an external field, resulting in a net dipole moment $\mathbf{m}$ (**Figure 9*a***). We distinguish two common types of magnetic particles—ferromagnetic and superparamagnetic—based on the dependence of their magnetic moment $\mathbf{m}$ on the applied field $\mathbf{H}$ (**Figure 9*b***). Ferromagnetic colloids have a permanent moment owing to the strong mutual alignment of their internal magnetic domains. By contrast, superparamagnetic colloids have a zero moment in the absence of an external field. In weak fields, the dipole moment is linearly proportional to the field as $\mathbf{m} = \chi V_{\text{p}}\mathbf{H}$, where χ is the susceptibility and V_{p} is the particle volume. In comparison to superparamagnetic composites ($\chi \sim 1$), the magnetic response of paramagnetic ($\chi = 10^{-5}$–10^{-2}) and diamagnetic materials ($\chi = -10^{-5}$) is weak; such materials are often approximated as nonmagnetic.

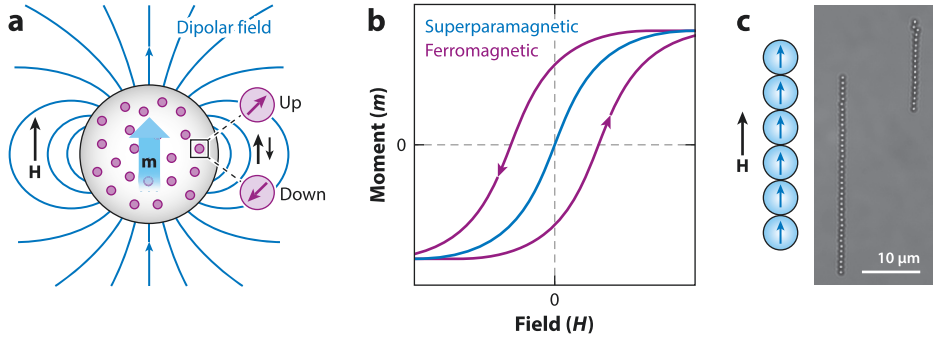

Figure 9

(*a*) Schematic illustration of a magnetic colloid containing magnetic domains that align in an external field **H**. (*b*) Plots of the magnetic moment *m* versus applied field strength *H* illustrate ferromagnetic and superparamagnetic responses. (*c*) Superparamagnetic particles assemble in a static field to form chains that minimize the dipolar interaction energy.

5.1.2. Magnetic dipolar interactions. To a first approximation, two magnetic colloids i and j interact via dipole–dipole interactions with the pair potential

$$U_{ij} = \frac{\mu_o}{4\pi}\left[\frac{\mathbf{m}_i \cdot \mathbf{m}_j}{r_{ij}^3} - \frac{3(\mathbf{m}_i \cdot \mathbf{r}_{ij})(\mathbf{m}_j \cdot \mathbf{r}_{ij})}{r_{ij}^5}\right], \quad 4.$$

where $\mathbf{r}_{ij}$ is the displacement vector between dipoles $\mathbf{m}_i$ and $\mathbf{m}_j$, and μ_0 is the magnetic permeability of free space. For ferromagnetic particles, the moments $\mathbf{m}_i$ and $\mathbf{m}_j$ are intrinsic properties of the particles, independent of the external field. By contrast, the dipole moments of superparamagnetic particles depend on the external field with additional contributions from the disturbance fields of neighboring particles. In the simplest dipolar model, these contributions are neglected, and the dipole moments are assumed to be proportional to the applied field. In this case, the interaction potential can be expressed more simply as a function of the angle θ between the displacement $\mathbf{r}_{ij}$ and the external field $\mathbf{H}_0$ as $U_{ij} \propto [1 - 3\cos^2(\theta)]$. The applied field strength acts as a knob to tune the magnitude of these interactions, which can be attractive ($U_{ij} < 0$) or repulsive ($U_{ij} > 0$) depending on θ. In a static field, such superparamagnetic colloids assemble to form linear chains with $\theta = 0$ that minimize the dipolar interaction energy (**Figure 9*c***). When the dipoles of neighboring particles are strongly coupled (i.e., when $\chi > 1$), the dipolar model is inadequate, and many-body interactions must be considered (81, 82).

5.2. Time-Varying Magnetic Fields

Time-varying fields act to modulate dipolar interactions and induce magnetic torques $\mathbf{T}_m = \mu_o(\mathbf{m} \times \mathbf{H})$ that drive particle rotation. By varying the field magnitude, frequency, and waveform, one observes various structures including colloidal chains, ribbons, membranes, networks, foams, and clusters (8, 83, 84).

5.2.1. Time-averaged dipolar interactions. For isotropic superparamagnetic colloids, the magnetic torque is often negligible because the dipole moment is nearly parallel to the magnetic field. For such particles, time-varying fields create oscillating energy landscapes that direct dynamic assemblies, which depend on the driving frequency ω relative to the particle diffusivity (e.g., $D_r = 1\ s^{-1}$ for 1 μm spheres in water) (85). When the driving frequency is fast (i.e., $\omega \gg D_r$), magnetic colloids interact primarily by time-averaged potentials. For example, consider a

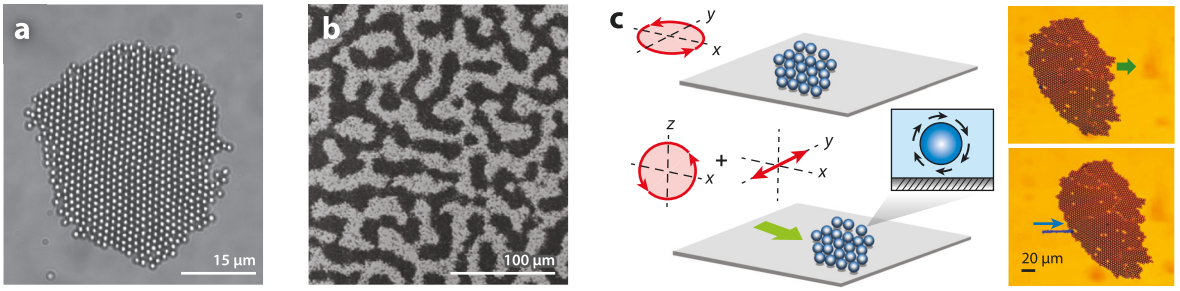

Figure 10

Assemblies of superparamagnetic colloids in time-varying magnetic fields. (*a*) Microscopy image shows a particle cluster assembled in the plane of a rotating magnetic field at 20 Hz and 11 G; the degree of crystallinity depends on the field strength. (*b*) Phase separation by spinodal decomposition is observed at higher particle density. (*c*) The schematic illustrates a suspension of superparamagnetic colloids clustering in a rotating magnetic field in the *xy* plane and then translating when the field is rotated in the *xz* plane. Microscopy images show the motion of these colloidal carpets at sequential time points. Panel *a* adapted from Reference 87. Panel *b* adapted from Reference 88. Panel *c* adapted from Reference 89 (CC BY 4.0).

collection of magnetic spheres in the *xy* plane subject to a rotating field with constant magnitude H_0 and angular velocity ω, $\mathbf{H}(t) = H_0[\cos(\omega t)\mathbf{e}_x + \sin(\omega t)\mathbf{e}_y]$. The time-averaged dipolar potential, $\langle U_{ij}\rangle \propto -H_0^2/r_{ij}^3$, describes long-ranged attraction proportional to the square of the applied field strength. These interactions drive phase separation of magnetic colloids to form dense crystalline and liquid phases in two dimensions (86, 87) (**Figure 10*a***). At higher particle fractions, colloidal assemblies are directed into phase-separating assemblies characteristic of spinodal decomposition (88) (**Figure 10*b***). As discussed below, these dynamic assemblies appear to reach near-equilibrium structures controlled by the time-averaged interaction potential.

5.2.2. Torque-driven particle rotation. Though neglected above, the application of nonreciprocal fields (e.g., rotating fields) to superparamagnetic colloids can result in time-averaged magnetic torques $\mathbf{T}_\mathrm{m} = \mu_\mathrm{o}\langle \mathbf{m} \times \mathbf{H}\rangle$ that drive particle rotation. Nonzero torques on superparamagnetic colloids derive from the finite rate of particle magnetization, which leads to a phase lag between the magnetic moment and the external field (90, 91). This magnetic torque is balanced by the viscous torque, which increases linearly with the angular velocity of the particle as $T_\mathrm{v} = -\xi_\mathrm{r}\Omega$, where ξ_r is the rotational friction coefficient. By combining time-averaged dipolar interactions and torque-driven particle rotation, one can assemble colloidal "carpets" that roll across a solid substrate due to a rotating field in the *xz* plane (89) (**Figure 10*c***). Such mobile assemblies persist only in the presence of the time-varying field and disassemble by Brownian motion when the external field is removed.

For ferromagnetic particles, rotating magnetic fields drive synchronous particle rotation at low frequencies $\omega < \mu_\mathrm{o} mH/\xi_\mathrm{r}$ (**Figure 11*a***). Above this step-out frequency, the phase lag between the magnetic moment and the applied field is no longer constant; the rotation rate fluctuates about a mean value that decreases with increasing frequency. Particle rotation perpendicular to a solid surface leads to "rolling" as a result of hydrodynamic coupling between the magnetic torque and the linear velocity (**Figure 11*b***). The direction of motion is dictated the rotating field. By contrast, larger particles with finite inertia can exhibit symmetry-breaking propulsion in the plane perpendicular to an oscillating field (94) (**Figure 11*c***).

5.2.3. Collective dynamics of spinners and rollers. Ferromagnetic "spinners" rotating parallel to the substrate and rollers rotating perpendicular to the substrate interact through long-ranged hydrodynamic interactions as well as magnetic dipole–dipole interactions. The relative magnitude

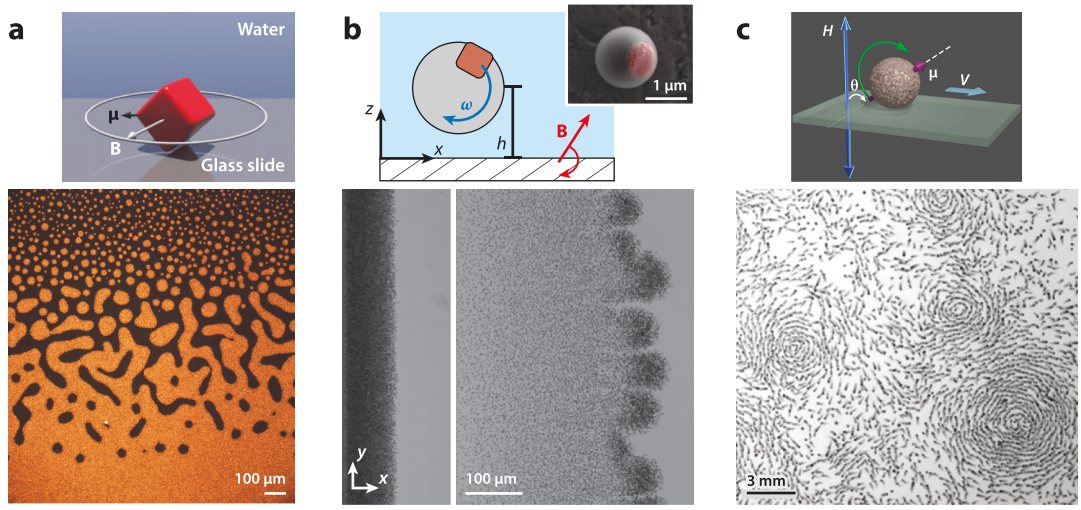

Figure 11

Emergent dynamics of ferromagnetic spinners and rollers. (*a*) Spinning hematite cubes form an active chiral fluid characterized by free surface flows and odd viscosity. (*b*) Rolling colloids embedded with a ferromagnetic cube form a moving front that exhibits a fingering instability due to hydrodynamic interactions. (*c*) Larger ferromagnetic particles (150 μm) roll in an oscillating field due to inertial effects and organize via hydrodynamic interactions to form rotating vortices. Panel *a* adapted from Reference 92. Panel *b* adapted from Reference 93. Panel *c* adapted from References 94 and 95.

of these competing interactions is characterized by a dimensionless Mason number. For spinning hematite cubes (92), the time-averaged dipolar interactions drive the condensation of a dense colloidal fluid in two dimensions (**Figure 11*a***). Hydrodynamic flows around each spinning particle drive the motion of their neighbors to produce steady particle currents concentrated near the interface of the colloidal fluid. Together, these hydrodynamic and dipolar interactions create an active chiral fluid that breaks both mirror and time-reversal symmetry, resulting in material properties such as odd viscosity prohibited in passive fluids.

Even when dipolar interactions are negligible, hydrodynamic interactions among rolling colloids can direct the formation of complex dynamic assemblies. Rotating magnetic fields drive moving fronts of colloidal rollers that undergo a fingering instability to form motile "critters" bound by hydrodynamic interactions (93) (**Figure 11*b***). For symmetry-breaking rollers powered by oscillating fields (94), hydrodynamic interactions mediate the formation of colloidal vortices in which particles roll along circular orbits to create flows that entrain their neighbors (95) (**Figure 11*c***). Mixtures of clockwise and counterclockwise vortices lead to enhanced mixing and transport reminiscent of that found in turbulent flows.

5.3. Pushing the Limits of Statistical Thermodynamics

Superparamagnetic colloids in time-varying magnetic fields provide a useful model with which to probe the limits of equilibrium descriptions of active colloids. Such colloids form gas, liquid, and solidlike phases due to time-averaged dipolar interactions in rotating magnetic fields (86, 96). The pair potential combines short-ranged electrostatic repulsion and long-ranged dipolar attraction to form magnetic "bonds" with strength $U_{\min} = 0.5\text{–}15\, k_B T$ set by the external field strength. By varying $U_{\min}$ and the particle density ϕ, the system can be used to construct phase diagrams showing gas–liquid and gas–solid coexistence curves (88, 96) (**Figure 12*a***). Equilibrium simulations based on the pair potential reproduce the phase boundaries observed in experiments

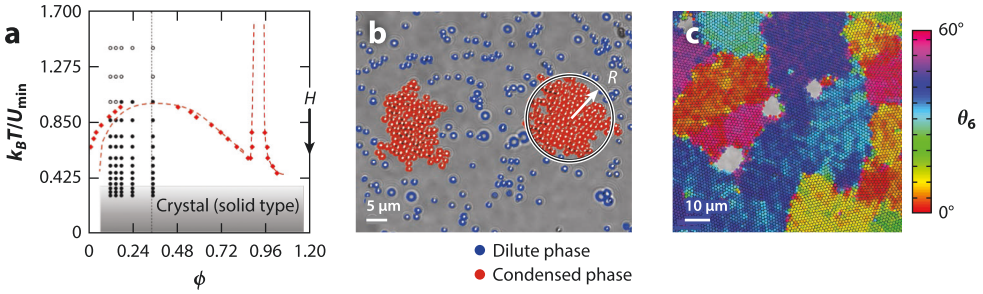

Figure 12

Superparamagnetic colloids in time-varying fields as models for statistical thermodynamics. (*a*) Temperature–density phase diagram for magnetic colloids in a rotating magnetic field. The interaction energy increases with increasing field strength as $U_{min} \propto H^2$. (*b*) Liquid–vapor coexistence shows fluctuations at the interface and particle exchange between dilute (*blue*) and condensed (*red*) phases. (*c*) Voids trapped within a colloidal crystal. The crystal orientation θ_6 shows ordered crystallites separated by grain boundaries. Panel *a* adapted from Reference 88. Panel *b* adapted from Reference 103. Panel *c* adapted from Reference 104.

(97). This agreement suggests that time-varying fields can direct the formation of equilibrium phases at high frequencies (here, 20 Hz) in the absence of applied torques. Magnetic colloids can therefore provide an experimental model for condensed matter, where tuning the magnetic interaction strength is analogous to changing the temperature (91, 98–100).

Colloidal models of vapor–liquid equilibrium can be used to investigate the statistical thermodynamics of the fluid interface. At equilibrium, the surface tension (here, line tension) of the interface is related to its thermal fluctuations, which grow with decreasing interaction strength. By quantifying these fluctuations for a flat interface, one can estimate the line tension and relate it to the strength of the magnetic interactions (101, 102). For small droplets of interacting particles, the highly curved interfaces act to increase the vapor pressure as described by the colloidal analog of the Kelvin equation (103). This relationship was established experimentally by analyzing the statistics of particles in liquid clusters and bulk gas (**Figure 12*b***).

The equilibrium description of magnetic colloids in time-varying fields can break down as a result of coupling between the oscillating interactions and the particle dynamics at lower frequencies and/or the presence of magnetic torques at higher frequencies. The effects of such torques are evident in studies of solid–gas coexistence, which show that particle voids act as both source and sink for grain boundaries (104). Ordered crystal domains and grain boundaries can be identified by the local bond-orientational order parameter θ_6 (**Figure 12*c***). From an equilibrium perspective, these grain boundaries are characterized by an energetic cost and should heal in time to reduce the free energy of the system. Instead, however, new grain boundaries appear as a result of interfacial shear due to the rotating magnetic field. New theoretical frameworks are required to understand and control the dynamics of colloidal materials with time-varying potentials and/or external torques.

6. ELECTRIC FIELD–DRIVEN COLLOIDS

Order parameters: measure the degree of order and are used to identify distinct phases

Like magnetic fields, electric fields act to polarize particles and the surrounding medium to induce dipolar interactions that influence the structure and dynamics of colloidal dispersions (105, 106). However, electric fields act also on charge present in the electrolyte and at the particle surface to drive dissipative currents and electrokinetic flows with no magnetic analog. These currents and flows provide a basis for active colloids that use self-propelled motions and nonconservative interactions to form dynamic assemblies. In this way, colloids driven by electric fields combine

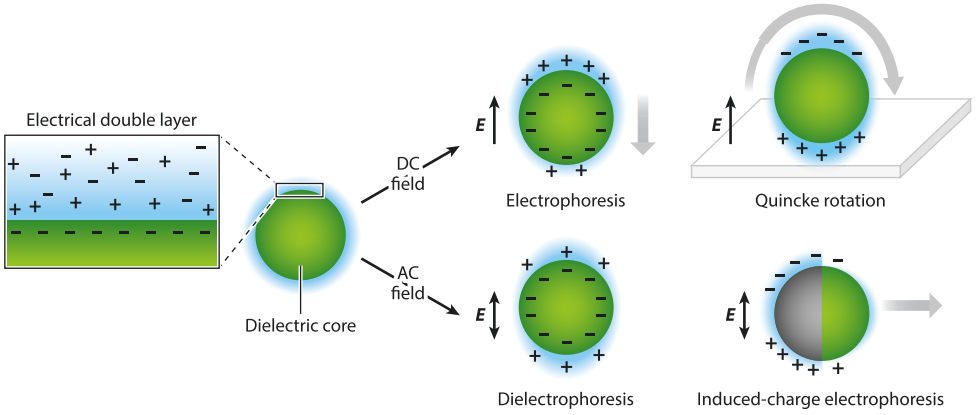

Figure 13

Schematic illustration of a colloidal sphere in static DC and time-oscillating AC electric fields. The field acts on charge bound to the particle surface (here, negative) as well as ionic charge in the surrounding electrolyte. Such fields act to polarize the double layer, induce fluid flows, and propel particle motions (*large gray arrows*) by different mechanisms.

the effects of time-varying potentials and nonconservative forces to produce a variety of complex nonequilibrium behaviors. This section provides a brief introduction to the different mechanisms of particle actuation in both static and time-oscillating electric fields and their potential to create active reconfigurable materials (**Figure 13**).

6.1. Static Direct Current Electric Field

DC electric fields induce steady ionic currents in liquid electrolytes that influence the motion of dispersed particles through different mechanisms, which depend on the applied field strength and on the properties of the two phases and their interface.

6.1.1. Electrophoresis. The application of a static electric field causes the directed migration of colloidal particles by electrophoresis (107, 108). The external field acts on the charged particle surface and the neutralizing counterions in the surrounding double layer to drive fluid flows. The resulting particle motion is force free and is directed parallel to the field for common conditions of thin double layers and/or isotropic particles. Despite its dissipative, force-free character, electrophoresis is rarely considered a form of self-propulsion because the direction of motion is dictated by the external field. By contrast, sufficiently high field strengths can lead to symmetry-breaking instabilities that provide a basis for active colloids in DC fields. When $E \gg k_B T/ea$ (e.g., 250 V/cm for $a = 1$ μm), nonlinear contributions due to field-induced charging of the particle surface can lead to rotation and translation perpendicular to the field in a electrokinetic analog of the Magnus effect (109).

6.1.2. Quincke rotation. Above a critical field strength, static fields can propel the steady rotation of insulating particles in conductive fluids due to the so-called Quincke instability. The applied field induces a dipolar charge distribution at the particle surface, which directs the flow of electric current around the particle. This dipole is directed antiparallel to the field and becomes unstable when the rate of particle rotation exceeds that of dipolar charging. For an insulating sphere in an unbounded fluid, the standard leaky dielectric model (110) predicts steady rotation for field strengths exceeding a critical value, $E_c = 8\eta/\tau\varepsilon_p$, where ε_p is the particle permittivity,

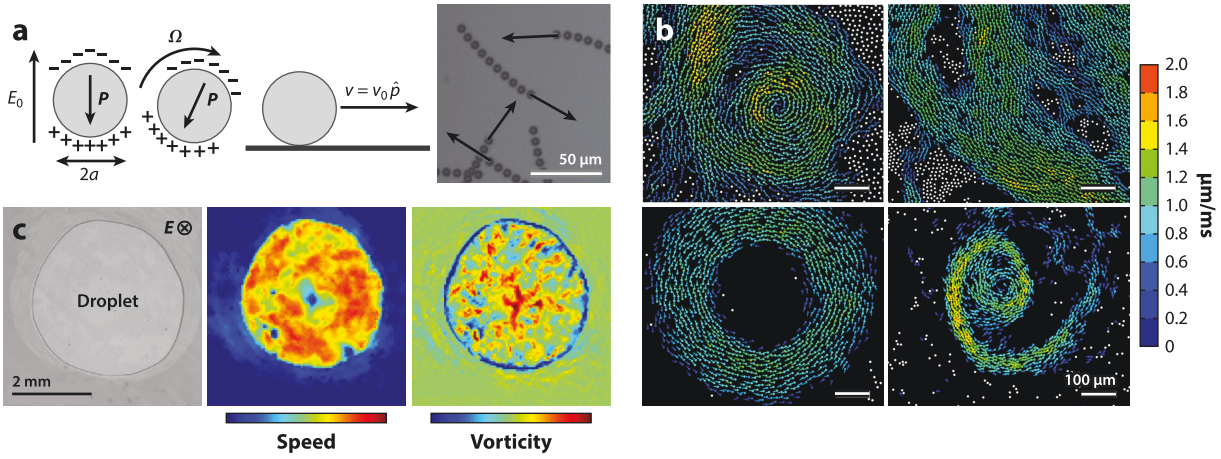

Figure 14

(*a*) Schematic showing Quincke rotation of a sphere in a DC field and corresponding microscope image showing the particle trajectories. (*b*) Collective dynamics of particles in a DC field below the threshold field strength required for Quincke rotation of isolated particles. (*c*) Image of a fluctuating droplet containing Quincke rollers. The velocity and vorticity plots show the fluid flows driving droplet deformation. Panel *a* adapted from Reference 113. Panel *b* adapted from Reference 114. Panel *c* adapted from Reference 115 (CC BY 4.0).

η is the fluid viscosity, and $\tau = \varepsilon/\sigma$ is the charge relaxation time (111, 112). In practice, this condition is realized in weakly conductive dielectric fluids (e.g., AOT–hexadecane mixtures), for which the critical field is less than the dielectric strength of the fluid. Quincke rotation above a planar electrode provides a basis for self-propelled rollers (113) that move in the plane perpendicular to the applied field (**Figure 14*a***).

Ensembles of colloidal rollers based on Quincke rotation form dynamic assemblies such as flocks and vortices as a result of hydrodynamic and electric interactions among the particles. Confined within a microfluidic racetrack, such Quincke rollers organize and move in a common direction reminiscent of bird flocks and fish schools (113). Hydrodynamic interactions between neighboring rollers act to synchronize and align particle rotation to produce polar liquids with suppressed velocity and density fluctuations. Once formed, the direction of such polar flocks can be reversed by a brief cessation and reapplication of the external field (116). Even below the critical field required for rolling, electrostatic interactions between neighboring particles can trigger the Quincke instability to produce activity waves and rotating vortices among other emergent patterns (114) (**Figure 14*b***). When confined by the deformable boundary of a liquid drop, Quincke rollers drive shape fluctuations, drop propulsion, and division due to two-way coupling between particle activity and drop shape (115) (**Figure 14*c***). At high field strengths, Quincke rollers can exhibit oscillatory back-and-forth motions that provide a basis for active matter with self-oscillating units (117).

6.2. Time-Varying Alternating Current Electric Field

AC electric fields with zero time average effectively eliminate linear DC effects such as electrophoresis, thereby isolating nonlinear electrokinetic phenomena such as dielectrophoresis and induced-charge electrophoresis (ICEP) that scale as the square of the applied field.

6.2.1. Dielectrophoresis. The application of an AC electric field to a colloidal particle creates an oscillating dipole due to the polarization of the particle core and its ionic double layer.

The magnitude and phase of this dipolar disturbance depend on the frequency of the driving field relative to the intrinsic relaxation time(s) for polarization. Electric field gradients induce time-averaged forces on such particles that drive their migration to or from regions of high field strength (118, 119). This process of positive or negative dielectrophoresis is useful for manipulating colloids and directing their assemblies (120, 121); however, such conservative forces are not a source of particle activity. By contrast, AC fields also produce fluid flows at the particle surface due to effects of the field on field-induced charge in the double layer (122, 123). These flows—known as induced-charge electro-osmosis—can be directed by particle asymmetries to propel the force-free motion of active colloids.

6.2.2. Induced-charge electrophoresis. Anisotropic particles exhibit self-propelled motions in AC electric fields known as ICEP (105, 124–126). In a pioneering study, metallodielectric Janus spheres were observed to propel themselves perpendicular to the applied field due to asymmetric flows induced on their respective hemispheres (124) (**Figure 15*a*,*b***). Like phoretic propulsion (Section 4.1.4), this and other ICEP motions are constrained by the symmetry of the particle. By contrast, the translational and rotational velocities now depend on the particle orientation with

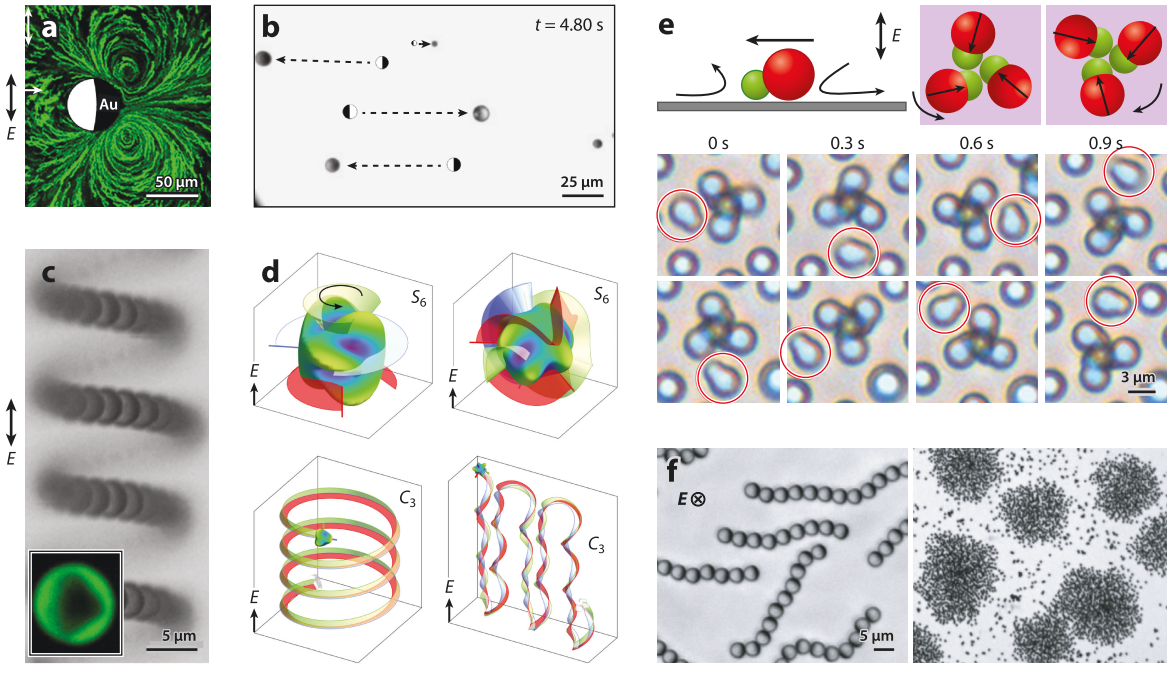

Figure 15

(*a*) Fluorescent microscope image showing motion of tracer particles in the electro-osmotic flow around a stationary Janus sphere in an AC electric field. (*b*) Active motion of Au-polystyrene metallodielectric Janus spheres in an AC electric field. (*c*) A microscope image showing the helical trajectory of a metallodielectric particle with a triangular patch (*inset*). (*d*) Nonlinear ICEP trajectories of model particles with shapes of different point symmetry. (*e*) Schematic and microscope images showing the active rotation of chiral clusters formed by asymmetric dimers in an out-of-plane electric field. (*f*) Microscope images of active assemblies and collective phases formed by Janus spheres in an AC electric field. Abbreviation: ICEP, induced-charge electrophoresis. Panel *a* adapted from Reference 122. Panel *b* adapted from Reference 124. Panel *c* adapted from Reference 128 (CC BY 4.0). Panel *d* adapted from Reference 54. Panel *e* adapted from Reference 130. Panel *f* adapted from Reference 131.

respect to the AC field as

$$\mathbf{U} = \frac{\varepsilon a}{\eta}\mathfrak{C} : \mathbf{EE} \quad \text{and} \quad \boldsymbol{\Omega} = \frac{\varepsilon}{\eta}\mathfrak{D} : \mathbf{EE}, \tag{5.}$$

where η and ε are the viscosity and permittivity of the fluid, respectively, and a is the particle radius (54, 127). The dimensionless tensors $\mathfrak{C}$ and $\mathfrak{D}$ share the symmetry of the particle and are uniquely specified by its shape and composition. In this way, particle asymmetries direct propulsion along complex nonlinear trajectories in three dimensions, as predicted theoretically (54) and later demonstrated experimentally (128, 129) (**Figure 15*c*,*d***). These motions can enhance the rates of particle transport within porous media, which may prove useful in the design of self-propelled microrobots (126).

Asymmetric particles propelled by ICEP interact with one another and with proximal boundaries through a combination of electrostatic, hydrodynamic, and phoretic interactions. Pear-shaped colloids swim across a planar electrode due to asymmetric electrokinetic flows induced at the solid–electrolyte interfaces (130). Additionally, dipole–dipole interactions among the particles direct their assembly into chiral clusters that rotate in a preferred direction determined by their handedness (**Figure 15*e***). Similarly, the imbalance of electrostatic interactions combined with hydrodynamic forces can direct the assembly of metallodielectric Janus particles into complex structures and phases (**Figure 15*f***). These dynamic assemblies can be designed by tuning the applied frequency and the ionic strength to control the balance among competing mechanisms of propulsion and interaction (131). Such tunable interactions have recently been applied in the context of microrobots, where Janus particles propelled by ICEP capture and release colloidal cargo on demand (132, 133).

7. FUTURE PERSPECTIVES

In the past decade, significant progress has been made in the synthesis and design of active colloids. The dynamic assembly of these dissipative systems continues to provide new insights into the fundamental principles underlying their collective behaviors. The next generation of active colloids, which will define the direction of research in the coming decade, will focus on three key areas, introduced above and discussed below—specifically, active colloids as models, materials, and machines. The continued development of these colloidal systems and their emergent behaviors will address questions and encounter challenges in areas of nonequilibrium thermodynamics, transport phenomena in living matter, and microrobotics.

7.1. Active Colloids as Models

As evidenced by the many examples above, active colloids are useful experimental models with which to discover and investigate the emergent behaviors of nonequilibrium, many-body systems. The purpose of such models is to reconcile, explain, and predict the observed macroscopic behaviors such as phase separation, self-assembly, and flocking in terms of the properties, interactions, and activity of their individual components. For systems that form equilibrium phases, the tools of thermodynamics and statistical mechanics provide a well-worn path between micro- and macroscopic descriptions spanning many scales in length and time. Under some (more limited) conditions, these concepts can be adapted to describe the macroscopic behaviors of active matter out of equilibrium using effective thermodynamic variables and potentials. The local validity of such approximations depends on the extent to which time-reversal symmetry is preserved for particular degrees of freedom over a specific range of length and timescales. Additional research is needed to determine if and when equilibrium descriptions are effective and to relate "effective"

thermodynamic quantities to particle-level dynamics. Experimental studies of active colloids—for example, field-driven phase separation of magnetic particles (Section 5.3)—can provide valuable insights in answering these questions.

Complementary to the thermodynamic perspective, hydrodynamic descriptions (134) based on conservation principles, symmetries, and constitutive relations provide an alternative framework by which to understand the macroscopic behaviors of active colloidal fluids. Recent experiments on chiral fluids formed by rotating ferromagnetic colloids exemplify this approach (92) (**Figure 11*a***). Due to the rotating field, the fluid breaks both parity and time-reversal symmetries (135). As a result, the hydrodynamic equations governing active chiral fluids contain new contributions, such as odd viscosity (135), which are absent from simple liquids. Evidence of these contributions is found in the spontaneous free-surface flows of rotating colloidal fluids (10, 92, 136). Related reports of odd elasticity (137) in crystals of self-rotating biocolloids (starfish embryos) further highlight the value of active colloids as model systems in elucidating new principles of nonequilibrium physics (138).

7.2. Active Colloids as Materials

Colloidal materials assembled from active components enable functional properties and behaviors that are difficult or impossible to achieve in their equilibrium counterparts. By breaking detailed balance, active materials are able to assemble and disassemble via different pathways, thereby offering greater control over structure and dynamics. Structures maintained by continuous energy dissipation can exhibit an improved ability to repair defects and heal damage. The kinetic stability of active assemblies allows for the coexistence of many stable structures and provides opportunities to reconfigure between them. In particular, materials that perform nonreciprocal deformations can exert stresses on their surroundings that drive work and/or motion. The dissipative processes that direct active assemblies introduce new length and timescales that can be used to encode material size and shape. The potential capabilities of active colloidal materials are best illustrated by the remarkable functions of living matter.

Despite their potential, it remains challenging to design and control active colloids to achieve targeted functions. The design space of possible building blocks and driving fields grows ever larger in pursuit of increasingly complex material behaviors. New strategies based on improved models, high-throughput experiments, and machine learning approaches are needed to navigate this space efficiently in search of functional designs. Meanwhile, experimental studies of active colloids based on simple building blocks serve to increase our understanding and inspire heuristic strategies for material design. The ability to manipulate external fields based on real-time sensing of particle position provides opportunities for feedback control over the structure and dynamics of colloidal materials (139). Given sensory information (e.g., from optical microscopy), learned control policies select the appropriate driving field to achieve functional objectives such as the assembly of defect-free crystals (140). Similar methods based on external sensing and actuation can be employed to design, create, and control active assemblies with targeted structures and dynamics.

7.3. Active Colloids as Machines

Active colloids provide a basis for microrobots that move through structured environments and cooperate to perform targeted functions (141). Arguably, the most advanced demonstrations of microrobots use magnetic particles driven and controlled by time-varying fields. Colloidal microwheels, assembled in situ from superparamagnetic components, can roll along blood vessel walls to disrupt clots (142, 143) (**Figure 16*a***). Linear assemblies of ferromagnetic cubes create field-responsive microgrippers that close and open to capture and release colloidal cargo (144)

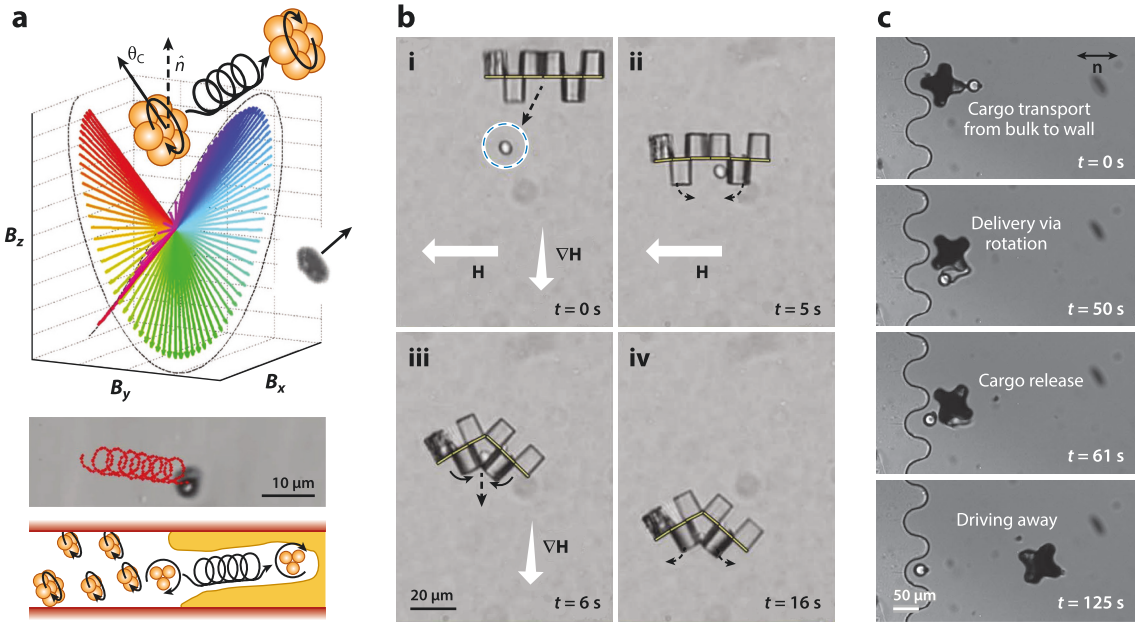

Figure 16

Examples of magnetic microrobots. (*a*) Rotating "corkscrew" fields are used to assemble colloidal microwheels that are capable of penetrating biopolymer networks responsible for blood clots. (*b*) Magnetic Janus cubes assemble into sequence-dependent robots that can act as microgrippers upon application of a static field. (*c*) A four-armed ferromagnetic microrobot in a nematic liquid crystal is propelled by a rotating field and responds to the nemato-elastic energy landscape of the liquid crystal. Panel *a* adapted from Reference 143. Panel *b* adapted from Reference 144. Panel *c* adapted from Reference 145.

(**Figure 16*b***). A four-armed magnetic microrobot in a nematic liquid crystal interacts with its local environment to transport cargo to targeted locations (145) (**Figure 16*c***). Swarms of ferromagnetic colloids use multiple driving fields to produce different modes of organization that enable them to perform multiple tasks such as navigating channels and transporting cargo (140).

Current microrobots are often controlled using external feedback mechanisms to direct their motion, like microscopic marionettes (146, 147). By contrast, primitive forms of sensing, actuation, and control can be encoded directly into the physicochemical dynamics of active colloids. Chemically fueled particles can navigate autonomously (i.e., without external control) by orienting their propulsion in response to local gradients in chemical concentration (148, 149), light intensity (150), and fluid velocity (151, 152), among other stimuli. The next generation of microrobots should incorporate dedicated sensing modalities to achieve greater awareness of their local environment (153). Conditioned on these sensory inputs, autonomous microrobots should be able to "decide" between multiple candidate responses—for example, stop, go, capture, and release. To this end, further research is needed to develop active colloids with primitive "brains" based on internal states and feedback mechanisms (154, 155). Finally, to act on their decisions, microrobots require multiple modes of actuation tailored to the task at hand—for example, swimming through the human body, navigating to a tumor site, and releasing a therapeutic payload (156).

Looking forward, ensembles of active particles can be used to build colloidal machines (11, 70) that blur the boundaries between materials and microrobots to create robots made of robots made of. . .colloids (157). This vision is inspired by living organisms in which mindless (but well-designed) molecular mechanisms such as motor proteins organize to form mindless (but

increasingly intelligent) assemblies such as the cytoskeleton that come together in a tangled hierarchy of cells and tissues to enable biological function. Such complex nonequilibrium machines provide evidence for the possible capabilities of active materials to move, repair, reconfigure, sense, compute, grow, and replicate. While the current capabilities of colloidal machines remain woefully primitive by comparison, their simplicity is also a strength, as it allows for a greater understanding of the emergent part–whole relationships. With patience and persistence, the study of these curious particles that move and interact with apparent purpose (158) will deepen our understanding of living matter and enhance our ability to engineer its synthetic analogs. With interdisciplinary training in thermodynamics, transport phenomena, chemical kinetics, and control theory, chemical engineers are uniquely well positioned to contribute to this growing field of active soft matter.

DISCLOSURE STATEMENT

The authors are not aware of any affiliations, memberships, funding, or financial holdings that might be perceived as affecting the objectivity of this review.

ACKNOWLEDGMENTS

K.J.M.B. acknowledges support from the Center for Bio-Inspired Energy Science, an Energy Frontier Research Center funded by the US Department of Energy, Office of Science, Basic Energy Sciences, under award DESC0000989. S.L.B. acknowledges financial support from the National Science Foundation under awards CBET-1705703 and TI-2141112. B.B. acknowledges financial support from the National Science Foundation under grants CBET-1943986 (NSF CAREER) and CBET-2038305.

LITERATURE CITED

1. Dou Y, Dhatt-Gauthier K, Bishop KJM. 2019. Thermodynamic costs of dynamic function in active soft matter. *Curr. Opin. Solid State Mater. Sci.* 23:28–40
2. Poon W. 2004. Colloids as big atoms. *Science* 304:830–31
3. Wang W, Duan W, Ahmed S, Mallouk TE, Sen A. 2013. Small power: autonomous nano- and micromotors propelled by self-generated gradients. *Nano Today* 8:531–54
4. Bechinger C, Di Leonardo R, Löwen H, Reichhardt C, Volpe G, Volpe G. 2016. Active particles in complex and crowded environments. *Rev. Mod. Phys.* 88:045006
5. Zhang J, Luijten E, Grzybowski BA, Granick S. 2017. Active colloids with collective mobility status and research opportunities. *Chem. Soc. Rev.* 46:5551–69
6. Han K, Shields CW IV, Velev OD. 2018. Engineering of self-propelling microbots and microdevices powered by magnetic and electric fields. *Adv. Funct. Mater.* 28:1705953
7. Palagi S, Fischer P. 2018. Bioinspired microrobots. *Nat. Rev. Mater.* 3:113–24
8. Spatafora-Salazar A, Lobmeyer DM, Cunha LHP, Joshi K, Biswal SL. 2021. Hierarchical assemblies of superparamagnetic colloids in time-varying magnetic fields. *Soft Matter* 17:1120–55
9. Sharko A, Livitz D, De Piccoli S, Bishop KJM, Hermans TM. 2022. Insights into chemically fueled supramolecular polymers. *Chem. Rev.* 122:11759–77
10. Nguyen NH, Klotsa D, Engel M, Glotzer SC. 2014. Emergent collective phenomena in a mixture of hard shapes through active rotation. *Phys. Rev. Lett.* 112:075701
11. Spellings M, Engel M, Klotsa D, Sabrina S, Drews AM, et al. 2015. Shape control and compartmentalization in active colloidal cells. *PNAS* 112:E4642–50
12. Nel AE, Mädler L, Velegol D, Xia T, Hoek E, et al. 2009. Understanding biophysicochemical interactions at the nano–bio interface. *Nat. Mater.* 8:543–57
13. Bishop KJM, Wilmer CE, Soh S, Grzybowski BA. 2009. Nanoscale forces and their uses in self-assembly. *Small* 5:1600–30

14. Grzelczak M, Vermant J, Furst EM, Liz-Marzán LM. 2010. Directed self-assembly of nanoparticles. *ACS Nano* 4:3591–605
15. He M, Gales JP, Ducrot É, Gong Z, Yi GR, et al. 2020. Colloidal diamond. *Nature* 585:524–29
16. Cademartiri L, Bishop KJM. 2015. Programmable self-assembly. *Nat. Mater.* 14:2–9
17. Zwanzig R. 2001. *Nonequilibrium Statistical Mechanics*. Oxford, UK: Oxford Univ. Press
18. Leyva SG, Stoop RL, Pagonabarraga I, Tierno P. 2022. Hydrodynamic synchronization and clustering in ratcheting colloidal matter. *Sci. Adv.* 8:eabo4546
19. Brady JF, Bossis G. 1988. Stokesian dynamics. *Annu. Rev. Fluid Mech.* 20:111–57
20. Glotzer SC, Solomon MJ. 2007. Anisotropy of building blocks and their assembly into complex structures. *Nat. Mater.* 6:557–62
21. Kim S, Karrila SJ. 2013. *Microhydrodynamics: Principles and Selected Applications*. Mineola, NY: Dover
22. Hunter GL, Weeks ER. 2012. The physics of the colloidal glass transition. *Rep. Prog. Phys.* 75:066501
23. Whitaker KA, Varga Z, Hsiao LC, Solomon MJ, Swan JW, Furst EM. 2019. Colloidal gel elasticity arises from the packing of locally glassy clusters. *Nat. Commun.* 10:2237
24. De Groot SR, Mazur P. 1984. *Non-Equilibrium Thermodynamics*. Mineola, NY: Dover
25. Reimann P. 2002. Brownian motors: noisy transport far from equilibrium. *Phys. Rep.* 361:57–265
26. Mewis J, Wagner NJ. 2012. *Colloidal Suspension Rheology*. Cambridge, UK: Cambridge Univ. Press
27. O'Brien RW, White LR. 1978. Electrophoretic mobility of a spherical colloidal particle. *J. Chem. Soc. Faraday Trans. 2* 74:1607–26
28. Velegol D, Garg A, Guha R, Kar A, Kumar M. 2016. Origins of concentration gradients for diffusiophoresis. *Soft Matter* 12:4686–703
29. Anderson JL. 1989. Colloid transport by interfacial forces. *Annu. Rev. Fluid Mech.* 21:61–99
30. Lauga E, Powers TR. 2009. The hydrodynamics of swimming microorganisms. *Rep. Prog. Phys.* 72:096601
31. Howse JR, Jones RA, Ryan AJ, Gough T, Vafabakhsh R, Golestanian R. 2007. Self-motile colloidal particles: from directed propulsion to random walk. *Phys. Rev. Lett.* 99:048102
32. O'Byrne J, Kafri Y, Tailleur J, van Wijland F. 2022. Time irreversibility in active matter, from micro to macro. *Nat. Rev. Phys.* 4:167–83
33. Kamdar S, Shin S, Leishangthem P, Francis LF, Xu X, Cheng X. 2022. The colloidal nature of complex fluids enhances bacterial motility. *Nature* 603:819–23
34. Paxton WF, Kistler KC, Olmeda CC, Sen A, St. Angelo SK, et al. 2004. Catalytic nanomotors: autonomous movement of striped nanorods. *J. Am. Chem. Soc.* 126:13424–31
35. Golestanian R, Liverpool T, Ajdari A. 2007. Designing phoretic micro- and nano-swimmers. *New J. Phys.* 9:126
36. Moran JL, Posner JD. 2017. Phoretic self-propulsion. *Annu. Rev. Fluid Mech.* 49:511–40
37. Ebbens S, Tu MH, Howse JR, Golestanian R. 2012. Size dependence of the propulsion velocity for catalytic Janus-sphere swimmers. *Phys. Rev. E* 85:020401
38. Ebbens S, Gregory DA, Dunderdale G, Howse JR, Ibrahim Y, et al. 2014. Electrokinetic effects in catalytic platinum-insulator Janus swimmers. *Eur. Phys. Lett.* 106:58003
39. Brown A, Poon W. 2014. Ionic effects in self-propelled Pt-coated Janus swimmers. *Soft Matter* 10:4016–27
40. Das S, Garg A, Campbell AI, Howse J, Sen A, et al. 2015. Boundaries can steer active Janus spheres. *Nat. Commun.* 6:8999
41. Simmchen J, Katuri J, Uspal WE, Popescu MN, Tasinkevych M, Sánchez S. 2016. Topographical pathways guide chemical microswimmers. *Nat. Commun.* 7:10598
42. Wu H, Greydanus B, Schwartz DK. 2021. Mechanisms of transport enhancement for self-propelled nanoswimmers in a porous matrix. *PNAS* 118:e2101807118
43. Campbell AI, Ebbens SJ, Illien P, Golestanian R. 2019. Experimental observation of flow fields around active Janus spheres. *Nat. Commun.* 10:3952
44. Golestanian R, Liverpool TB, Ajdari A. 2005. Propulsion of a molecular machine by asymmetric distribution of reaction products. *Phys. Rev. Lett.* 94:220801
45. Córdova-Figueroa UM, Brady JF. 2008. Osmotic propulsion: the osmotic motor. *Phys. Rev. Lett.* 100:158303

46. Uspal W, Popescu MN, Dietrich S, Tasinkevych M. 2015. Self-propulsion of a catalytically active particle near a planar wall: from reflection to sliding and hovering. *Soft Matter* 11:434–38
47. Mozaffari A, Sharifi-Mood N, Koplik J, Maldarelli C. 2016. Self-diffusiophoretic colloidal propulsion near a solid boundary. *Phys. Fluids* 28:053107
48. Prieve DC, Anderson JL, Ebel JP, Lowell ME. 1984. Motion of a particle generated by chemical gradients. Part 2. Electrolytes. *J. Fluid Mech.* 148:247–69
49. Zhou X, Wang S, Xian L, Shah ZH, Li Y, et al. 2021. Ionic effects in ionic diffusiophoresis in chemically driven active colloids. *Phys. Rev. Lett.* 127:168001
50. Brown AT, Poon WCK, Holm C, De Graaf J. 2017. Ionic screening and dissociation are crucial for understanding chemical self-propulsion in polar solvents. *Soft Matter* 13:1200–22
51. Brooks AM, Tasinkevych M, Sabrina S, Velegol D, Sen A, Bishop KJM. 2019. Shape-directed rotation of homogeneous micromotors via catalytic self-electrophoresis. *Nat. Commun.* 10:495
52. Wang Y, Hernandez RM, Bartlett DJ, Bingham JM, Kline TR, et al. 2006. Bipolar electrochemical mechanism for the propulsion of catalytic nanomotors in hydrogen peroxide solutions. *Langmuir* 22:10451–56
53. Wang W, Chiang TY, Velegol D, Mallouk TE. 2013. Understanding the efficiency of autonomous nano- and microscale motors. *J. Am. Chem. Soc.* 135:10557–65
54. Brooks AM, Sabrina S, Bishop KJM. 2018. Shape-directed dynamics of active colloids powered by induced-charge electrophoresis. *PNAS* 115:E1090–99
55. Kirvin A, Gregory D, Parnell A, Campbell AI, Ebbens S. 2021. Rotating ellipsoidal catalytic microswimmers via glancing angle evaporation. *Mater. Adv.* 2:7045–53
56. Wykes MSD, Zhong X, Tong J, Adachi T, Liu Y, et al. 2017. Guiding microscale swimmers using teardrop-shaped posts. *Soft Matter* 13:4681–88
57. Katuri J, Caballero D, Voituriez R, Samitier J, Sanchez S. 2018. Directed flow of micromotors through alignment interactions with micropatterned ratchets. *ACS Nano* 12:7282–91
58. Michelin S, Lauga E. 2014. Phoretic self-propulsion at finite Péclet numbers. *J. Fluid Mech.* 747:572–604
59. Maass CC, Krüger C, Herminghaus S, Bahr C. 2016. Swimming droplets. *Annu. Rev. Condens. Matter Phys.* 7:171–93
60. Michelin S. 2023. Self-propulsion of chemically active droplets. *Annu. Rev. Fluid Mech.* 55:77–101
61. Soto R, Golestanian R. 2014. Self-assembly of catalytically active colloidal molecules: tailoring activity through surface chemistry. *Phys. Rev. Lett.* 112:068301
62. Soto R, Golestanian R. 2015. Self-assembly of active colloidal molecules with dynamic function. *Phys. Rev. E* 91:052304
63. Nasouri B, Golestanian R. 2020. Exact phoretic interaction of two chemically active particles. *Phys. Rev. Lett.* 124:168003
64. Varma A, Michelin S. 2019. Modeling chemo-hydrodynamic interactions of phoretic particles: a unified framework. *Phys. Rev. Fluids* 4:124204
65. Palacci J, Sacanna S, Steinberg AP, Pine DJ, Chaikin PM. 2013. Living crystals of light-activated colloidal surfers. *Science* 339:936–40
66. Niu R, Palberg T, Speck T. 2017. Self-assembly of colloidal molecules due to self-generated flow. *Phys. Rev. Lett.* 119:028001
67. Niu R, Fischer A, Palberg T, Speck T. 2018. Dynamics of binary active clusters driven by ion-exchange particles. *ACS Nano* 12:10932–38
68. Schmidt F, Liebchen B, Löwen H, Volpe G. 2019. Light-controlled assembly of active colloidal molecules. *J. Chem. Phys.* 150:094905
69. Meredith CH, Moerman PG, Groenewold J, Chiu YJ, Kegel WK, et al. 2020. Predator–prey interactions between droplets driven by non-reciprocal oil exchange. *Nat. Chem.* 12:1136–42
70. Aubret A, Martinet Q, Palacci J. 2021. Metamachines of pluripotent colloids. *Nat. Commun.* 12:6398
71. Wysocki A, Winkler RG, Gompper G. 2014. Cooperative motion of active Brownian spheres in three-dimensional dense suspensions. *Eur. Phys. Lett.* 105:048004
72. Agudo-Canalejo J, Golestanian R. 2019. Active phase separation in mixtures of chemically interacting particles. *Phys. Rev. Lett.* 123:018101

73. Cates ME, Tailleur J. 2015. Motility-induced phase separation. *Annu. Rev. Condens. Matter Phys.* 6:219–44
74. Redner GS, Hagan MF, Baskaran A. 2013. Structure and dynamics of a phase-separating active colloidal fluid. *Phys. Rev. Lett.* 110:055701
75. Buttinoni I, Bialké J, Kümmel F, Löwen H, Bechinger C, Speck T. 2013. Dynamical clustering and phase separation in suspensions of self-propelled colloidal particles. *Phys. Rev. Lett.* 110:238301
76. Takatori SC, Yan W, Brady JF. 2014. Swim pressure: stress generation in active matter. *Phys. Rev. Lett.* 113:028103
77. Solon AP, Fily Y, Baskaran A, Cates ME, Kafri Y, et al. 2015. Pressure is not a state function for generic active fluids. *Nat. Phys.* 11:673–78
78. Solon AP, Stenhammar J, Wittkowski R, Kardar M, Kafri Y, et al. 2015. Pressure and phase equilibria in interacting active Brownian spheres. *Phys. Rev. Lett.* 114:198301
79. Takatori SC, Brady JF. 2015. Towards a thermodynamics of active matter. *Phys. Rev. E* 91:032117
80. Fialkowski M, Bishop KJ, Klajn R, Smoukov SK, Campbell CJ, Grzybowski BA. 2006. Principles and implementations of dissipative (dynamic) self-assembly. *J. Phys. Chem. B* 110:2482–96
81. Du D, Toffoletto F, Biswal SL. 2014. Numerical calculation of interaction forces between paramagnetic colloids in two-dimensional systems. *Phys. Rev. E* 89:043306
82. Du D, Biswal SL. 2014. Micro-mutual-dipolar model for rapid calculation of forces between paramagnetic colloids. *Phys. Rev. E* 90:033310
83. Martin JE, Snezhko A. 2013. Driving self-assembly and emergent dynamics in colloidal suspensions by time-dependent magnetic fields. *Rep. Prog. Phys.* 76:126601
84. Tierno P, Snezhko A. 2021. Transport and assembly of magnetic surface rotors. *ChemNanoMat* 7:881–93
85. Swan JW, Bauer JL, Liu Y, Furst EM. 2014. Directed colloidal self-assembly in toggled magnetic fields. *Soft Matter* 10:1102–9
86. Du D, Li D, Thakur M, Biswal SL. 2013. Generating an *in situ* tunable interaction potential for probing 2-D colloidal phase behavior. *Soft Matter* 9:6867–75
87. Hilou E, Du D, Kuei S, Biswal SL. 2018. Interfacial energetics of two-dimensional colloidal clusters generated with a tunable anharmonic interaction potential. *Phys. Rev. Mater.* 2:025602
88. Hilou E, Joshi K, Biswal SL. 2020. Characterizing the spatiotemporal evolution of paramagnetic colloids in time-varying magnetic fields with Minkowski functionals. *Soft Matter* 16:8799–805
89. Massana-Cid H, Meng F, Matsunaga D, Golestanian R, Tierno P. 2019. Tunable self-healing of magnetically propelling colloidal carpets. *Nat. Commun.* 10:2444
90. Janssen X, Schellekens A, Van Ommering K, van IJzendoorn L, Prins M. 2009. Controlled torque on superparamagnetic beads for functional biosensors. *Biosens. Bioelectron.* 24:1937–41
91. Klapp SH. 2016. Collective dynamics of dipolar and multipolar colloids: from passive to active systems. *Curr. Opin. Colloid Interface Sci.* 21:76–85
92. Soni V, Bililign ES, Magkiriadou S, Sacanna S, Bartolo D, et al. 2019. The odd free surface flows of a colloidal chiral fluid. *Nat. Phys.* 15:1188–94
93. Driscoll M, Delmotte B, Youssef M, Sacanna S, Donev A, Chaikin P. 2017. Unstable fronts and motile structures formed by microrollers. *Nat. Phys.* 13:375–80
94. Kaiser A, Snezhko A, Aranson IS. 2017. Flocking ferromagnetic colloids. *Sci. Adv.* 3:1601469
95. Han K, Kokot G, Tovkach O, Glatz A, Aranson IS, Snezhko A. 2020. Emergence of self-organized multivortex states in flocks of active rollers. *PNAS* 117:9706–11
96. Du D, Doxastakis M, Hilou E, Biswal SL. 2017. Two-dimensional melting of colloids with long-range attractive interactions. *Soft Matter* 13:1548–53
97. Kryuchkov NP, Smallenburg F, Ivlev AV, Yurchenko SO, Löwen H. 2019. Phase diagram of two-dimensional colloids with Yukawa repulsion and dipolar attraction. *J. Chem. Phys.* 150:104903
98. Yethiraj A. 2007. Tunable colloids: control of colloidal phase transitions with tunable interactions. *Soft Matter* 3:1099–115
99. Wang M, He L, Yin Y. 2013. Magnetic field guided colloidal assembly. *Mater. Today* 16:110–16
100. Imperio A, Reatto L, Zapperi S. 2008. Rheology of colloidal microphases in a model with competing interactions. *Phys. Rev. E* 78:021402
101. Tüzel E, Pan G, Kroll DM. 2010. Dynamics of thermally driven capillary waves for two-dimensional droplets. *J. Chem. Phys.* 132:174701

102. Goldstein RE, Jackson DP. 1994. Domain shape relaxation and the spectrum of thermal fluctuations in Langmuir monolayers. *J. Phys. Chem.* 98:9626–36
103. Joshi K, Biswal SL. 2022. Extension of Kelvin's equation to dipolar colloids. *PNAS* 119:e2117971119
104. Lobmeyer DM, Biswal SL. 2022. Grain boundary dynamics driven by magnetically induced circulation at the void interface of 2D colloidal crystals. *Sci. Adv.* 8:eabn5715
105. Diwakar NM, Kunti G, Miloh T, Yossifon G, Velev OD. 2022. AC electrohydrodynamic propulsion and rotation of active particles of engineered shape and asymmetry. *Curr. Opin. Colloid Interface Sci.* 59:101586
106. Harraq AA, Choudhury BD, Bharti B. 2022. Field-induced assembly and propulsion of colloids. *Langmuir* 38:3001–16
107. Hunter RJ. 2001. *Foundations of Colloid Science*. Oxford, UK: Oxford Univ. Press
108. Khair AS. 2022. Nonlinear electrophoresis of colloidal particles. *Curr. Opin. Colloid. Interface Sci.* 59:101587
109. Sherman ZM, Swan JW. 2020. Spontaneous electrokinetic Magnus effect. *Phsy. Rev. Lett.* 124:208002
110. Saville DA. 1997. Electrohydrodynamics: the Taylor-Melcher leaky dielectric model. *Annu. Rev. Fluid Mech.* 29:27–64
111. Jones TB. 1984. Quincke rotation of spheres. *IEEE Trans. Ind. Appl.* 20:845–49
112. Das D, Saintillan D. 2013. Electrohydrodynamic interaction of spherical particles under Quincke rotation. *Phys. Rev. E* 87:043014
113. Bricard A, Caussin JB, Desreumaux N, Dauchot O, Bartolo D. 2013. Emergence of macroscopic directed motion in populations of motile colloids. *Nature* 503:95–98
114. Liu ZT, Shi Y, Zhao Y, Chaté H, Shi XQ, Zhang TH. 2021. Activity waves and freestanding vortices in populations of subcritical Quincke rollers. *PNAS* 118:e2104724118
115. Kokot G, Faizi HA, Pradillo GE, Snezhko A, Vlahovska PM. 2022. Spontaneous self-propulsion and nonequilibrium shape fluctuations of a droplet enclosing active particles. *Commun. Phys.* 5:91
116. Zhang B, Yuan H, Sokolov A, de la Cruz MO, Snezhko A. 2022. Polar state reversal in active fluids. *Nat. Phys.* 18:154–59
117. Zhang Z, Yuan H, Dou Y, De La Cruz MO, Bishop KJM. 2021. Quincke oscillations of colloids at planar electrodes. *Phys. Rev. Lett.* 126:258001
118. Jones TB. 1995. *Electromechanics of Particles*. Cambridge, UK: Cambridge Univ. Press
119. Bharti B, Findenegg GH, Velev OD. 2014. Analysis of the field-assisted permanent assembly of oppositely charged particles. *Langmuir* 30:6577–87
120. Bharti B, Velev OD. 2015. Multidirectional, multicomponent electric field driven assembly of complex colloidal chains. *Z. Phys. Chem.* 229:1075–88
121. Bharti B, Velev OD. 2015. Assembly of reconfigurable colloidal structures by multidirectional field-induced interactions. *Langmuir* 31:7897–908
122. Peng C, Lazo I, Shiyanovskii SV, Lavrentovich OD. 2014. Induced-charge electro-osmosis around metal and Janus spheres in water: patterns of flow and breaking symmetries. *Phys. Rev. E* 90:051002
123. Bazant MZ, Squires TM. 2004. Induced-charge electrokinetic phenomena: theory and microfluidic applications. *Phys. Rev. Lett.* 92:066101
124. Gangwal S, Cayre OJ, Bazant MZ, Velev OD. 2008. Induced-charge electrophoresis of metallodielectric particles. *Phys. Rev. Lett.* 100:058302
125. Bazant MZ. 2011. Induced-charge electrokinetic phenomena. In *Electrokinetics and Electrohydrodynamics in Microsystems*, ed. A Ramos, pp. 221–97. Berlin: Springer
126. Al Harraq A, Bello M, Bharti B. 2022. A guide to design the trajectory of active particles: from fundamentals to applications. *Curr. Opin. Colloid Interface Sci.* 61:101612
127. Yariv E. 2005. Induced-charge electrophoresis of nonspherical particles. *Phys. Fluids* 17:051702
128. Lee JG, Brooks AM, Shelton WA, Bishop KJM, Bharti B. 2019. Directed propulsion of spherical particles along three dimensional helical trajectories. *Nat. Commun.* 10:2575
129. Lee JG, Al Harraq A, Bishop KJM, Bharti B. 2021. Fabrication and electric field-driven active propulsion of patchy microellipsoids. *J. Phys. Chem. B* 125:4232–40
130. Ma F, Wang S, Wu DT, Wu N. 2015. Electric-field–induced assembly and propulsion of chiral colloidal clusters. *PNAS* 112:6307–12

131. Yan J, Han M, Zhang J, Xu C, Luijten E, Granick S. 2016. Reconfiguring active particles by electrostatic imbalance. *Nat. Mater.* 15:1095–99
132. Wu Y, Fu A, Yossifon G. 2021. Micromotor-based localized electroporation and gene transfection of mammalian cells. *PNAS* 118:e2106353118
133. Wu Y, Fu A, Yossifon G. 2020. Active particles as mobile microelectrodes for selective bacteria electroporation and transport. *Sci. Adv.* 6:eaay4412
134. Marchetti MC, Joanny JF, Ramaswamy S, Liverpool TB, Prost J, et al. 2013. Hydrodynamics of soft active matter. *Rev. Mod. Phys.* 85:1143–89
135. Banerjee D, Souslov A, Abanov AG, Vitelli V. 2017. Odd viscosity in chiral active fluids. *Nat. Commun.* 8:1573
136. Yeo K, Lushi E, Vlahovska PM. 2015. Collective dynamics in a binary mixture of hydrodynamically coupled microrotors. *Phys. Rev. Lett.* 114:188301
137. Scheibner C, Souslov A, Banerjee D, Surówka P, Irvine W, Vitelli V. 2020. Odd elasticity. *Nat. Phys.* 16:475–80
138. Tan TH, Mietke A, Li J, Chen Y, Higinbotham H, et al. 2022. Odd dynamics of living chiral crystals. *Nature* 607:287–93
139. Tang X, Grover MA. 2022. Control of microparticle assembly. *Annu. Rev. Control Robot. Auton. Syst.* 5:491–514
140. Zhang J, Yang J, Zhang Y, Bevan MA. 2020. Controlling colloidal crystals via morphing energy landscapes and reinforcement learning. *Sci. Adv.* 6:eabd6716
141. Li J, Rozen I, Wang J. 2016. Rocket science at the nanoscale. *ACS Nano* 10:5619–34
142. Tasci TO, Herson PS, Neeves KB, Marr DWM. 2016. Surface-enabled propulsion and control of colloidal microwheels. *Nat. Commun.* 7:10225
143. Tasci TO, Disharoon D, Schoeman RM, Rana K, Herson PS, et al. 2017. Enhanced fibrinolysis with magnetically powered colloidal microwheels. *Small* 13:1700954
144. Han K, Shields CW IV, Diwakar NM, Bharti B, López GP, Velev OD. 2017. Sequence-encoded colloidal origami and microbot assemblies from patchy magnetic cubes. *Sci. Adv.* 3:1701108
145. Yao T, Kos V, Zhang QX, Luo Y, Serra F, et al. 2022. Nematic colloidal micro-robots as physically intelligent systems. *Adv. Funct. Mater.* 32:2205546
146. Miskin MZ, Cortese AJ, Dorsey K, Esposito EP, Reynolds MF, et al. 2020. Electronically integrated, mass-manufactured, microscopic robots. *Nature* 584:557–61
147. Brooks AM, Strano MS. 2020. A conceptual advance that gives microrobots legs. *Nature* 584:530–31
148. Hong Y, Blackman NM, Kopp ND, Sen A, Velegol D. 2007. Chemotaxis of nonbiological colloidal rods. *Phys. Rev. Lett.* 99:178103
149. Popescu MN, Uspal WE, Bechinger C, Fischer P. 2018. Chemotaxis of active Janus nanoparticles. *Nano Lett.* 18:5345–49
150. Lozano C, Ten Hagen B, Löwen H, Bechinger C. 2016. Phototaxis of synthetic microswimmers in optical landscapes. *Nat. Commun.* 7:12828
151. Palacci J, Sacanna S, Abramian A, Barral J, Hanson K, et al. 2015. Artificial rheotaxis. *Sci. Adv.* 1:e1400214
152. Sharan P, Xiao Z, Mancuso V, Uspal WE, Simmchen J. 2022. Upstream rheotaxis of catalytic Janus spheres. *ACS Nano* 16:4599–608
153. Dou Y, Bishop KJM. 2019. Autonomous navigation of shape-shifting microswimmers. *Phys. Rev. Res.* 1:032030
154. Alvarez L, Fernandez-Rodriguez MA, Alegria A, Arrese-Igor S, Zhao K, et al. 2021. Reconfigurable artificial microswimmers with internal feedback. *Nat. Commun.* 12:4762
155. van Kesteren S, Alvarez L, Arrese-Igor S, Alegria A, Isa L. 2022. Self-propelling colloidal finite state machines. arXiv:2208.03003 [cond-mat.soft]
156. Chowdhury S, Castro S, Coker C, Hinchliffe TE, Arpaia N, Danino T. 2019. Programmable bacteria induce durable tumor regression and systemic antitumor immunity. *Nat. Med.* 25:1057–63
157. Savoie W, Berrueta TA, Jackson Z, Pervan A, Warkentin R, et al. 2019. A robot made of robots: emergent transport and control of a smarticle ensemble. *Sci. Robot.* 4:eaax4316
158. Venkatasubramanian V, Sivaram A, Das L. 2022. A unified theory of emergent equilibrium phenomena in active and passive matter. *Comput. Chem. Eng.* 164:107887

Annual Review of Chemical and Biomolecular Engineering

Volume 14, 2023

Contents

Errata

An online log of corrections to *Annual Review of Chemical and Biomolecular Engineering* articles may be found at http://www.annualreviews.org/errata/chembioeng